Dalton Transactions

Accepted Manuscript

ROYAL SOCIETY OF CHEMISTRY

www.rsc.org/dalton

Luminescent pentafluorophenyl-cycloplatinated complexes: synthesis, characterization, photophysics, cytotoxicity and cellular imaging

J. R. Berenguer,[a] J. G. Pichel,*[b] N. Giménez,[a] E. Lalinde,[a] M. T. Moreno,*[a] S. Piñeiro-Hermida.[b]

[a]*Departamento de Química-Centro de Síntesis Química de La Rioja, (CISQ), Universidad de La Rioja, 26006, Logroño, Spain. E-mail: teresa.moreno@unirioja.es*

[b]*Centro de Investigación Biomédica de La Rioja (CIBIR), Fundación Rioja Salud, 26006, Logroño, Spain. E-mail: jgpichel@riojasalud.es*

Abstract

Luminescent mono(pentafluorophenyl) cycloplatinated complexes [Pt(C^N-κ*C*,*N*)(HC^N-κ*N*)(C_6F_5)] [HC^N = Hthpy (2-(2-thienyl)pyridine) **2a**, Hbt (2-phenylbenzothiazole**)** **2b**, Hpq (2-phenylquinoline) **2c**] have been prepared by C-H activation of a HC^N ligand in the corresponding [Pt(HC^N-κ*N*)$_2$(C_6F_5)$_2$] (**1a**, **1b**, **1c**) complexes. Complexes **2** evolve in DMSO solution to the solvate complexes and we present here successful routes for the synthesis of [Pt(C^N)(C_6F_5)(DMSO)] (C^N = thphy **3a**, bt **3b**). They have been fully characterized (X-ray for **1a**, **1c**, **2b**, **3a** and **3b**), their electronic absorption and emission properties investigated and DFT and TD-DFT calculations for **1a**, **1c**, **2b** and **3a** carried out. Complexes **3a**, **3b** and [Pt(ppy)(C_6F_5)(DMSO)] **4** (Hppy = 2-phenylpiridine) show remarkable stability in mixed DMSO-cellular medium and their cytotoxicity towards the human lung tumor (A549) and bronchial epithelial non-tumorigenic (NL20) cell lines has been evaluated by MTS assay. Their cellular localization in A549 and NL20 human cells and in mouse embryonic fibroblasts obtained from lungs (LMEFs) has been also investigated by fluorescent microscopy.

Introduction

Cisplatin and other platinum-based anticancer drugs are widely used to treat the cancer.[1] However, acquired resistance and unpleasant side effects[2] have led to an increasing interest in the development of other types of platinum-based drugs. In this context, cyclometalated compounds containing Pt(II) have revealed promising anticancerous activities.[3] Due to the presence of a $\sigma(Pt\text{-}C)_{cylometalated}$ bond, these complexes are quite stable, and therefore would be more likely they reach the cell unaltered. Furthermore, the aromatic cyclometalated units could favor the DNA-binding intercalation through $\pi^{\cdots}\pi$ staking.[4] Finally, the introduction of auxiliary labile ligands in the cyclometalated Pt fragment could induce covalent coordination to DNA (as for cisplatin), with substitution rates comparable to those of many cellular division processes.[5] All these factors (cyclometalation, intercalation and labile positions) produce a combined effect that result in a great interest on their therapeutic potential. The cytotoxicities of several platinum compounds containing bidentate (C^N) or terdentate (C^N^N) ligands have been studied.[3]

Moreover, cyclometalated Pt(II) complexes have shown variable molecular structure, intense absorption and tunable emission in the visible region with high luminescent quantum yields and long emission lifetimes,[6] and in some cases they are cell-permeable and surprisingly photostable. As a consequence, phosphorescent cycloplatinated complexes are also gaining attention as luminescent labels for bioimaging.[7] To date, several kinds of simple bidentate (C^N) and tridentate (N^C^N, C^N^N) platinum complexes,[7a, 7d, 7g, 8] exceptionally encapsulated inside polymeric particles or micelles,[7a, 9] have been successfully applied as bioimaging probes. In order to rationally design novel drugs or complexes with potential applications as bioimaging agents, the study of the chemical structure-internalization relationship is still a challenging goal.

We and others have recently described some luminescent pentafluorophenyl cyclometalated Pt derivatives.[10] In these complexes, the presence of strong Pt-C_6F_5 bonds not only increases their stability but also significantly improves their emission properties in solution. Previously we reported that the *in situ* formed bis(pentafluorophenyl) bis(N^CH) complex [*cis*-$Pt(Hbzq)_2(C_6F_5)_2$] (Hbzq = 7,8-benzoquinoline) undergoes a fast C-H metalation in CH_2Cl_2 to yield the cyclometalated

luminescent complex [Pt(bzq)(Hbzq)(C_6F_5)] and in acetone the solvate [Pt(bzq)(C_6F_5)(acetone)].[10a] This solvate has been recently used to prepare unusual η^2-alkyne complexes[10a] or interesting heterometallic Pt_2M clusters (M = Pb,[11] Ag[10d]) featuring vapochromic responses. We thought that neutral [Pt(C^N)(C_6F_5)L] (L = labile ligand) systems could also show interesting biological properties. The lack of information on the biological activity of this kind of compounds prompted us to undertake the present study. Continuing with our interest in these systems, we report herein the synthesis, characterization and photophysics of new [Pt(HC^N-κ*N*)$_2$(C_6F_5)$_2$] [HC^N = Hthpy (2-(2-thienyl)pyridine) **1a**, Hbt (2-phenylbenzothiazole**) 1b**, Hpq (2-phenylquinoline) **1c**] complexes, which undergo subsequent C-H activation giving rise to final cyclometalated complexes [Pt(C^N-κ*C*,*N*)(HC^N-κ*N*)(C_6F_5)] (C^N = thpy **2a**, bt **2b**, pq **2c**). We had envisaged that these new complexes would exhibit desirable absorption and emission in solution under ambient conditions to be used in biological labelling studies. Studying their properties, we found that these **2a-c** complexes undergo a fast displacement reaction with the donor S(O)Me_2 molecule in dimethylsulphoxide solvent, which is the most widely used for laboratory-based preclinical studies. We have found only successful routes for the preparation of the corresponding solvate complexes [Pt(C^N)(C_6F_5)(DMSO)] (C^N = thpy **3a**, bt **3b**). The cytotoxicity of the complexes **3a** and **3b** together with the previously prepared by us [Pt(ppy)(C_6F_5)(DMSO)] **4** (ppy = phenylpyridine)[11b] towards human lung cancer (A549) and non-tumorigenic bronchial epithelial (NL20) cells has been examined by MTS assays. Furthermore, as these complexes are strongly emissive, their cellular localization has been investigated by fluorescent microscopy.

Results and Discussion

Synthesis and Characterization. Keeping with our previously described two-step process to prepare the cyclometalated complex [Pt(bzq)(Hbzq)(C_6F_5)],[10a] we tried this same procedure employing 2-(2-thienyl)pyridine (Hthpy), 2-phenylbenzothiazole (Hbt) and 2-phenylquinoline (Hpq) as N^CH ligands. Thus, as shown in Scheme 1i, [*cis*-Pt(C_6F_5)$_2$(THF)$_2$] was reacted with 2 equiv of the corresponding N^CH ligand in mild conditions (CH_2Cl_2, 1.5 to 5 h, room temperature) to give the bis(N^CH) derivatives [Pt(HC^N-κ*N*)$_2$(C_6F_5)$_2$] (**1a-c**). The anchoring of both N^CH ligands through the nitrogen

atom to the platinum center will allow subsequent C-H activation to afford new cyclometalated species. However, these systems require drastic conditions. In fact, **1a-c** only evolve to the monocyclometalated derivatives [Pt(C^N-κ*C,N*)(HC^N-κ*N*)(C_6F_5)] (**2a-c**) in refluxing xylene for 2h (Scheme 1ii).

With the goal of studying the cytotoxicity of the cyclometalated compounds **2a**, **2b** and **2c** in DMSO, we examined the stability of these compounds in DMSO-*d6* by ^{1}H NMR. Unfortunately, we found that by dissolving **2a-c** in DMSO, the N^CH ligand is easily substituted by a molecule of DMSO, giving rise the corresponding DMSO solvate [Pt(C^N)(C_6F_5)(DMSO)] (C^N = thpy **3a**, bt **3b**). This behavior should be taken into account when studying the biological activity of related complexes in DMSO. In the case of **2c**, a complex mixture of species was formed, in which the expected **3c** is also present. By this reason, we decided to prepare the DMSO solvates. As is shown in Scheme 1iii, complex **3a** is also formed, as an orange microcrystalline solid, in a similar way to that described for **4**,[11b] by reaction of [*cis*-Pt(C_6F_5)$_2$(DMSO)$_2$] with 1 equiv. of Hthpy in refluxing xylene. Unfortunately, attempts to prepare the corresponding bt or pq solvates by this route resulted unsuccessful, due to considerable decomposition to platinum. Complex **3b** was prepared, as a white solid, by refluxing **2b** in the minimum amount of DMSO for 4h (see Experimental for details, Scheme 1 iv). All attempts to isolate **3c** as a pure complex have been fruitless. As is confirmed in the X-ray structures of **3a** and **3b** (see below), the DMSO molecule is κ-*S* coordinated, in accordance with the softer character of the S in relation to the O atom. Taking into account the HSAB (hard and soft acids and bases) concept,[12] both Pt(II) and sulfur are concerned to be "soft" and are therefore expected to form stable bonds, whereas the harder Pt(IV) center shows mainly κ-*O* coordination, although examples with κ-*S* coordination are also known.[13]

These new compounds were fully and unambiguously characterized by multinuclear NMR spectroscopic analysis. All experiments were recorded in $CDCl_3$ and the signals were assigned on the basis on ^{1}H-^{1}H and ^{1}H-^{13}C correlation experiments (see Experimental Section and Fig. 1 and S1, S2†). For the bis(N^CH) derivatives **1**, the ^{1}H, ^{19}F and ^{13}C{^{1}H} NMR spectra confirm the presence of only one set of signals for both ligands (N^CH and C_6F_5). In the case of complexes **2**, both the metalated C^N and N^CH ligands are observed, whereas in the solvate complexes **3a** and **3b**, only the signals of the deprotonated C^N ligand are present. By comparison, the ^{1}H NMR spectra

of the thienylpyridine complexes **1a**, **2a** and **3a** and the free ligand are collected in Fig. 1 and commented in the text with more detail.

The thienyl derivative **1a** shows a doublet at δ 8.50, attributed to the H^{11} proton, deshielded as consequence of the close proximity to the Pt center, experiencing the anisotropic effect associated to the Pt dz^2 electron density.[10a] The signal at δ 7.90 with platinum satellites ($^3J_{Pt\text{-}H}$ = 28 Hz) is due to the H^2 proton adjacent to the N atom. The H^3 proton appears upfield shifted (δ 6.69), probably due to its proximity to the thienyl and C_6F_5 rings (Fig. 1). The ^{1}H NMR spectrum of **2a** is more complex. Notably, the $H^{2'}$ proton of the C^N ligand appears clearly downfield (δ 9.19) and the $H^{10'}$, adjacent to the metalated carbon, upfield shifted (δ 6.46), both with platinum satellites (25 and 26 Hz, respectively). The strong shielding of this signal is due to its proximity to the diamagnetic current of the C_6F_5 group, thus supporting the *cis* disposition of the C-metalated to the C_6F_5 group. By comparison, in the solvate complex **3a**, the $H^{2'}$ proton appears downfield shifted (δ 9.46), whereas the $H^{10'}$ is upfield (δ 6.04), both showing platinum satellites (28.5 and 27 Hz). It is worth mentioning that the $^3J_{Pt\text{-}H}$ values found for the *ortho* protons to the Pt-C (~26 Hz) in the thienyl derivatives are lower than those found for similar protons in complexes **2b**,**c** and **3b** (or **4**) (~ 65 Hz), featuring orthometalated phenyl rings. Comparison of the ^{1}H NMR spectra of the phenylbenzothiazolyl derivatives (bt) **2b** and **3b** in relation to that of **1b** (Fig. S1† and Experimental Section) confirms the presence of one cyclometalated ligand. The most distinctive signals are those of protons in the *ortho* position to the Pt-N (δ $H^{7'}$ 9.12 **2b**, 9.05 **3b**) and Pt-C (δ $H^{11'}$ 6.75 **2b**, 6.35 **3b**), respectively, these latter with a high Pt-H coupling constant (68 **2b**, 63 Hz **3b**). The remarkable steric congestion due to the coordination of two bulky Hpq ligands in **1c** is reflected in the *ortho* ($H^{9,9'}$) and *meta* ($H^{10,10'}$) proton signals of the phenyl ring, which are broad and close to coalescence at room temperature and split into four different resonances at 223 K (see Fig. S2†), evidencing that the phenyl ring is rigid on the NMR time scale. The congestion is also reflected in the ^{19}F NMR spectra, which are consistent with relatively rigid molecules not only for complexes **1** (for **1a** at -45ºC, see Fig. S3†) but also for cyclometalated complexes **2**, exhibiting five distinct signals, thus indicating that the rotation of the C_6F_5 ring around the Pt-C_{ipso} bond is hindered due to the steric hindrance of the HC^N ligands.

Molecular structures

The structures of complexes **1a**, **1c**, **2b**, **3a** and **3b** were stablished by X-ray diffraction studies. Fig. 2, 3 and 4 show views of the corresponding complexes and Table 1 lists a selection of relevant bond lengths. Complexes **1a** and **1c**·0.75 CH_2Cl_2 show a distorted planar environment for the platinum, formed by two *cis* non-chelated thienylpyridine (**1a**) or phenylquinoline (**1c**) ligands and two C_6F_5 rings ($Pt_2N_2C_2$). The HC^N ligands adopt a *transoidal* (or *anti*) disposition in relation to the platinum square planar, with dihedral angles between the pyridine groups and the Pt coordination planes of ~55º. The HC^N ligands are not planar, exhibiting in **1a** interplanar angles between the pyridine group and the thiazoline ring of 38.16º, 39.79º and in **1c** between the phenyl and quinoline groups of 64.72º and 59.13º. In **1a**, one of the thienyl ligands locates the C-H proton (H16) towards the platinum atom but with a long distance (3.044 Å). In **1c**, the H14 and H29 protons of the quinoline unit are placed in a pseudoaxial position above and below the platinum coordination plane, with a deviation of Pt-H14 and Pt-H29 vectors from the normal to this plane of ~58º. The Pt-H14/H29 2.772/2.759 Å distances are shorter than the sum of the van der Waals radii,[14] and the bond distances Pt-C14/C29 3.292/3.270 Å and angles Pt-H14-C14/Pt-H29-C29 116.31/115.63º fall within the range of the Pt···H bonding interactions reported in the literature.[10a, 15] The molecules stack showing weak secondary additional non-classic hydrogen contacts and in **1a** also π···π interactions (3.36 Å) (Fig. S4-S5†).

The structure of **2b** confirms the C-H activation of one of the HC^N (bt^-) ligands and the N-coordination of the other one (Hbt) (Fig. 3, Table 1). This compound represents one of the few Pt(II) complexes containing a chelated and a non-chelated cyclometalated ligand whose crystal structure has been determined.[10a, 16] In accordance with its spectroscopic data, the C_6F_5 ligand is in a *cis* position with respect to the metalated (C9) atom. The structural data are similar to those found for [Pt(bzq)(Hbzq)(C_6F_5)].[10a] The Pt-N2 is longer [2.152(3) Å] than Pt-N1 [2.101(3) Å], reflecting the high *trans* influence of the metalate carbon. The Hbt pendant ligand is coordinated almost perpendicular to the Pt coordination plane (dihedral angle 83.49º), locating the H22 and H15 protons close to Pt center (2.587 and 2.786 Å, respectively), suggesting the presence of Pt···H bonding interactions.[10a, 15] The molecules are arranged as dimers through moderate intermolecular π···π (Hbt···Hbt) (3.31 Å) and S···C(Hbt)

(3.50 Å) interactions and the dimers form chains mainly supported by similar offset π···π (Hbt···Hbt) interactions (3.35 Å) (Fig. S6†).

The solvate complexes **3a** and **3b** (Fig. 4, Table 1) exhibit a distorted planar environment due to the small bite angle of the NC cyclometalated ligand [79.0(3)º **3a**, 80.1(2) **3b**], with the C_6F_5 group coordinated in a *cis*-position in relation to the metalated carbon atom. The DMSO molecule shows the expected S coordination for Pt(II) derivatives,[17] with a Pt-S distance in both complexes [2.296(2) Å **3a**, 2.3140(13) **3b**] slightly larger than the average of this distance in related structures.[17-18] Complex **3a** stablishes a supramolecular arrangement through π···π intermolecular interactions of the cyclometalated thpy groups (minimum distance 3.340 Å), with secondary additional weak non-classic hydrogen contacts (Fig. S7†), whereas **3b** only shows intermolecular contacts involving fluorine atoms from C_6F_5 (Fig. S8†).

Photophysical Properties

Absorption Spectra. UV-vis absorption spectra were recorded for all complexes in CH_2Cl_2 and MeCN and the data are summarized in Table 2. The spectra of the thpy series together with that of the free ligand are shown in Fig. 5 and the corresponding spectra for the bt and pq series in Fig. S9†. The high energy intense absorptions are attributed to π-π* intraligand (^{1}IL, HC^N, C^N, C_6F_5) transitions. For complexes **1**, and according to the results of theoretical calculations, the intense bands, that follow the tendency of the free ligands (292 **1b**, 302 **1a**, 338 nm **1c**), bear a remarkable intraligand ^{1}IL' (HC^N) with some ligand to ligand (C_6F_5→HC^N) in **1a** or Pt to ligand charge transfer ^{1}ML'CT (Pt→HC^N) in **1c**. These complexes exhibit tails of very low intensity ascribed to ^{1}ML'CT (Pt→HC^N) transitions with some ^{1}IL' (HC^N) contribution. Complexes **2** and **3** exhibit a characteristic low energy feature (350-430 nm, ε = 9.7-0.8 x 10^3 $M^{-1}cm^{-1}$) typical of cycloplatinated systems, which is attributed (TD-DFT on **2b**, **3a**) to admixture of ^{1}IL (C^N) with metal to ligand (Pt→C^N) ^{1}MLCT contribution, higher in complexes **2**. This low energy band exhibits solvatochromic shift by increasing the polarity of the solvent (from CH_2Cl_2 to MeCN, Table 2), evidencing some charge transfer nature. The solvatochromism is negative in **2** indicating that the ground state is more polar than the excited state, whereas is positive in **3**, likely due to different contribution of the auxiliary ligand (HC^N in **2** and DMSO in **3**) to the ground state. The position of the low energy band follows the order thpy (**a**) > bt (**b**) > pq (**c**)

for complexes **2**, whereas the change of the C^N has very little effect in complexes **3**. As is observed in Fig. 5 and S9†, substitution of HC^N for DMSO causes a blue shift in the low energy absorption, indicating a decreased HOMO energy level.

Emission spectra. The emission data are compiled in Table 3. Complexes **1-3** exhibit long lived luminescence in degassed CH_2Cl_2 solution with similar profiles in general at 5×10^{-5}, 10^{-4} M and 10^{-3} M, being excitation-wavelength independent, indicating that aggregates are not responsible for the obtained spectra. In the solid state, they show bright emission at room temperature and at 77 K, except **3a** in solid state at 298 K. Complexes **1a** and **1c** show in fluid degassed solution (CH_2Cl_2) structured emissions blue-shifted in relation to that of the solid state (490 nm, τ 0.9 μs **1a**; 485 nm τ 0.6 (32%), 3.3 (68%) μs **1c**, Fig. S10†). For complex **1b** bearing the Hbt ligand, fluorescence located on the 2-phenylbenzothiazole Hbt group [370 nm, τ 120 (53%), 20 (47%) ns] and a broad low energy phosphorescence centered at 540 nm (τ 2 μs) was observed by exciting in the tail of the low energy absorption (λ < 350 nm), suggesting that the intersystem crossing is not very effective in this complex at 298 K. However, in the frozen matrix (77 K), all **1a-c** complexes exhibit highly structured emissions with minor differences in the maxima (506 **1a**, 475 nm **1b**,**c**) (Fig. 6). On the basis of theoretical calculations on **1a** and **1c** (see below), the emissions are attributed to a metal to ligand ^{3}ML'CT (Pt→H^CN) excited state with some ^{3}IL (HC^N) contribution. The solid samples of these complexes (HC^N-κ*N*)$_2$ **1** present in all cases a red-shifted (516-565 nm) broad emission profile at 298 K (slightly structured for **1c**), which become more structured at 77 K (Fig. S11†), attributed to solid state effects. Emission lifetimes are in the order of microseconds (12.8-102.8 μs, 298 K), increasing at 77 K (Table 3). It should be noted that for **1a** and **1c** the shape of the emission band depends on the crystallization conditions. Fig. S12† shows the emission profiles of different solid samples of **1a** (Fig. S12a†) or **1c** (Fig. S12b†) at 298 K: bulk material, ground solid and crystals obtained from CH_2Cl_2/*n*-hexane. For example, for **1a**, the *as-obtained* white solid shows an orange emission with two different and overlapped structured bands (520 and 560 nm) associated to different excitation spectra, thus suggesting the presence of at least two emitting luminophores, probably due to conformational isomerism of the two bulky HC^N coordinated ligands. It is reasonable to think that the two bulky coordinated N-ligands could generate different conformational isomers, a fact

previously described for cycloplatinated systems.[10b, 10e, 19] When the bulk material is finely ground and dried vacuum, the high energy peak at 520 nm essentially disappears, exhibiting only the structured band with a maximum at 560 nm. However, the few white crystals of **1a** obtained (CH_2Cl_2/*n*-hexane) display a yellow emission with a broad profile centered at 538 nm (Table 3). All of these characteristics and the observed large Stokes shifts, are indicative of phosphorescent emissions from excited states of essentially intraligand ^{3}IL character.

The cyclometalated complexes **2a-c** exhibit highly structured spectra in all media (Fig. 7 and Fig. S13-S14†). Profiles and emission lifetimes are typical of excited states of mixed ^{3}IL and ^{3}MLCT character, with high Pt contribution to the HOMO through the Pt-C bond formed. The emission maxima are, in general, red shifted in relation to the *bis*(HC^N) derivatives (**1**) (see for example, values in frozen CH_2Cl_2 : 550 **2a**, 515 **2b**, 548 **2c** *vs* 506 **1a**, 475 nm **1b**,**c**) and are dependent on the cyclometalated ligand decreasing in the order **2b** (*bt*) > **2a** (*thpy*) ~ **2c** (*pq*) in accordance with the energy gap of the ligands. Theoretical calculations on **2b** (see below) allow us to ascribe the emission in CH_2Cl_2 to intraligand ^{3}IL (C^N) excited state mixed with some metal to ligand charge transfer ^{3}MLCT (Pt→ C^N) contribution.

Substitution of the bulky ligands in **2a**,**b** for the small DMSO ligand in **3a**,**b** has a negative impact in their properties. Thus, complex **3a** is not emissive in the solid state at 298 K, a fact which is attributed to an aggregation quenching effect, probably because of intermolecular interactions related to $\pi^{\cdots}\pi$ contacts between the planar cyclometalated thpy units, as observed in solid state for **3a** (note the difference in the crystal packing of **3b**). Complex **3b** displays a yellow-orange emission (538, 298 K; 545 nm 77 K) but the quantum yield decreases notably in relation to **2b** (ϕ 2.5% **3b**, 16.5% **2b**). At 77 K both complexes display intense vibronically structured emissions with long lifetimes (64.1 μs **3a**, 26.0 μs **3b**, Fig. S15a†) indicative of an emitting state of notable ^{3}IL (C^N) character, also supported by theoretical calculations on **3a** (see below). In accordance of this assignment, as in series **2**, the phosphorescent emission for the phenylbenzothiazolyl derivative **3a** is red shifted in relation to **3b** (*i.e* 545 **3a** *vs* 525 nm **3b**, frozen CH_2Cl_2, Fig. S15b†). In fluid and frozen degassed CH_2Cl_2 solution, complex **3b** exhibits similar structured emission to that of **2b**, while **3a** shows at 298 K the phosphorescent emission (550, 595 nm, τ 8.5 μs Fig. 8), together with an unstructured fluorescent emission band at a high energy [435 nm, τ 5.2 (59%), 110

(41%) ns], probably of excimeric origin, in view of its small Stokes shift, the shape and the fact that no quenching was observed upon exposure to air. This pattern suggests that the intersystem crossing is not very effective in this complex at 298 K, probably due to the weaker Pt-Cmetalate bond.

Theoretical calculations

To get a better understanding of the photophysical properties of these complexes, we have carried out DFT and TD-DFT calculations for **1a**, **1c**, **2b** and **3a**. The bond distances an angles of the optimized geometries (S_0 and T_1, Table S1 and Fig. S16†) are in good agreement with those obtained by X-ray, although in **1a**, **1c** and **2b** the Pt···H (HC^N) contacts are shorter (**1a**, **1c**) or longer (**2b**) with respect to the experimental X-ray values. Diagrams of the frontier orbitals in the ground state of the four calculated complexes in CH_2Cl_2 are represented in the Fig. S17-S20† and the corresponding partial molecular orbital compositions in Table S2†. Excitation energies at the ground state geometry were calculated by TD-DFT in CH_2Cl_2 solution and selected low-lying transitions are provided in Table S3†. The calculated singlet excitations are in good qualitative agreement with the experimental absorption spectra (Fig. 9).

For complexes **1a** and **1c**, the target orbitals LUMO to LUMO+3 are distributed over both HC^N ligands (Hthpy **1a**, Hpq **1c**), whereas the HOMO is primarily located in the Pt center (73% **1a**, 82% **1c**) with some HC^N (21% **1a**, 10% **1c**). The lowest energy singlet transition calculated in CH_2Cl_2 (375 **1a**, 400 nm **1c**) arises primarily from HOMO to LUMO transition. Therefore, they are attributed to ^{1}ML'CT (Pt→H^CN) with some intraligand ^{1}IL' (H^CN) transitions. The most intense singlet excitations (Table S3†) correspond to transitions largely of ^{1}IL' (H^CN) with some ^{1}L''L'CT (C_6F_5→H^CN) in **1a** [308 nm (S_9)] and with some ^{1}ML'CT (Pt→H^CN) in **1c** [334 nm (S_7)].

For the cyclometalated complexes **2b** and **3a**, the lowest energy absorption (S_0-S_1 395 **2b**, 374 nm **3a**, Fig. 9) are in agreement with the tendency found experimentally in CH_2Cl_2 (420 **2b**, 398 nm **3a**). In both complexes, the absorption is derived primarily (contribution 84% **2b**, 94% **3a**) from the HOMO→LUMO transition. The HOMOs have mixed π bt (**2b**) or thpy (**3a**) and d(π)Pt (35% **2b**, 14% **3a**) character and the LUMOs are predominantly on the π* orbitals of the corresponding cyclometalated ligands (bt

91% **3b**, thpy 89% **3a**). Thus, the S_1 state can be described to have mixed ^{1}IL/^{1}MLCT character, but the contribution of the ^{1}MLCT is notably lower in the solvate derivatives.

We also investigated their emitting behavior by optimization of the lowest energy triplet state (T_1) using the unrestricted U-B3LYP method (Table S4†, Fig. 10). The calculated electronic energies with respect to the ground state (629 **1a**, 568 **1c**, 625 **2b**, 669 nm **3a**) are red shifted from to the experimental values (490 **1a**, 485 **1c**, 530 **2b**, 550 nm **3a**, CH_2Cl_2) due to insufficient description of the charge-transfer transitions using DFT calculations. For complexes **1a** and **1c**, the SOMO is essentially analogous to the LUMO in the ground state, although now it is only located on one H^CN, and the SOMO-1 is similar to the HOMO in the ground state, located on the Pt (74% **1a**, **1c**) and the H^CN ligand (18% **1a**, 12% **1c**). Therefore, the emission in **1a** and **1c** is due to a ^{3}ML'CT (Pt→H^CN) excited state with some ^{3}IL' (HC^N) contribution. For **2b** and **3a**, the SOMO orbitals in the optimized T_1 state are mainly centered, as the LUMO, on the C^N ligand (bt 95% **2b**, thpy 95% **3a**), whereas the SOMO-1 are similar to the HOMO orbitals, distributed on the C^N ligand (75% **2b**, 78% **3a**) and the Pt (23% **2b**, 20% **3a**), thus supporting a ^{3}IL (C^N) mixed with some ^{3}MLCT origin for their emission.

Biological assays

In order to assess the effect of DMSO and cellular medium on the activity of complexes **3a**, **3b** and **4**, their stability in these media was studied. The stability of the complexes in DMSO was performed in DMSO-*d6* solutions by ^{1}H NMR studies, observing that the compounds show identical spectra after 15 days at 298 K. By other hand, the investigated compounds were dissolved in DMSO (16mM **3a**, **4**; 8 mM **3b**) and their solution behaviour in cellular medium was analysed through UV-vis absorption spectroscopy. The experimental conditions to record adequate absorption spectra (50 μM in RPMI 1640 medium as used in MTS assays) are in the range to those employed for activity investigations, maintaining the DMSO content ≤ 1%. Representative spectral data for **3a**, **3b** and **4** are shown in Fig. S21†. From spectra inspection, it emerges that the Pt chromophores manifest a remarkable stability with the time with no evidence of changes even over a period of 96h [sufficiently long for them to reach their biological target (72h)].

Cytotoxicity tests (MTS Assay). We have examined the in vitro anti-cancer properties of the newly synthesized DMSO compounds **3a**, **3b** and **4** towards human lung cell lines A549 (tumoral adenocarcinomic alveolar basal epithelial cells) and NL20 (non-tumorigenic immortalized bronchial epithelial cells), by means of (3-(4,5-dimethylthiazol-2-yl)-5-(3-carboxymethoxyphenyl)-2-(4-sulfophenyl)-2H-tetrazolium) hydrolysis method (MTS assay). The cytotoxicity of cisplatin was also examined as a reference. The IC_{50} values were determined after cellular exposure to compounds for 72h (Table 4 and Fig. S22†). Cisplatin IC_{50} dose towards A549 cells (6.45 μM) was similar to that recently reported.[20] Complexes **3a**, **3b** and **4** were found to display similar anti-cancer activity towards these cells, although showing between 3 or 4 times less cytotoxic activity than cisplatin (24.70, 23.46 and 18.92 μM, respectively). When tested in the NL20 non-tumorigenic cells, these complexes showed approximately double cytotoxic activity (IC_{50} values of 10.45, 11.13 and 9.03 μM, respectively). Similarly, cisplatin showed the same ratio of increased cytotoxicity towards this cell line (IC_{50}: 2.83 μM). It is important to notice that **3a**, **3b** and **4** showed steeper curve falls of cytotoxicity with rising concentrations when compared to cisplatin, an effect observed in both cell lines (Fig. S22†). These results indicate a highly homogeneous response towards these compounds, and may suggest different cytotoxic mechanism of action compared to cisplatin. Shallow concentration-response relationships were previously interpreted as a sign of multiple cellular targets,[21] and therefore, could explain the higher cytotoxic activity of cisplatin in these cells.

Fluorescent microscopic cellular localization. In view of the favourable emission properties of **3a**, **3b** and **4** complexes, their potential as contrast agents was assessed.[22] To this aim, the compounds were incubated at concentrations of 40 μM, both alone (as control) and in combination with the DNA binder Hoechst 33258 (3.2 μM), with A549 and NL20 human cells and with immortalized mouse embryonic fibroblasts obtained from lungs (LMEFs) for 30 min. Living cell preparations were examined with a fluorescence microscope[7f, 23] suitable for alternate imaging with Nomarski DIC transmitted light, and with green, red and blue fluorescent emitted light. Superimposition of images obtained with Nomarski visualization and Hoechst staining of nuclear DNA helped to ascertain the site of fluorescence at subcellular levels. Results of cellular localization of **3a, 3b** and **4** are shown in Fig. 11 and S23†, and summarized in Table 4. We did not find any of the complexes showing blue light emission, spectral

region where Hoechst 33258 bound to DNA is visible (λ_{em} 461 nm)[24] and vice versa, Hoechst stain did not show emission bleeding in green and red channels, when their stains were performed separately (data not shown). However, we noticed that the three complexes showed the same pattern of cell staining when they were observed in green and red channels, but with a higher intensity in the green region (Fig. S23†, and data not shown), according to their spectral profiles. Complexes **3a** and **4** showed brighter cell staining than **3b**, effect that could be caused by differential fluorescent emission enhancement due to interaction with specific molecular environment. Staining in different inner cell compartments indicates that cell membranes are permeable to these compounds, and demonstrate that they can be traced in living cells using emission microscopy. It was previously noticed that DMSO increases cellular permeability to cisplatin that could be mediated by DMSO facilitation of platinum-protein binding.[25] It is possible that presence of DMSO in the structure of complexes **3a**, **3b** and **4** would help their cellular internalization. Although the three complexes stained the cytoplasm, with brighter emission in the perinuclear area, there were subtle differences among them, and between cell lines. Thus, **3a** and **4** additionally stained nucleoli in both human cell lines and LMEFs, and the rest of the nucleus with variable intensity in A549 and LMEFs (Fig. 11 A-H; Fig S23†). Interestingly, **3a** strongly marked nuclei with condensed DNA in A549 cells, as revealed its co-localization with the highest levels of Hoechts staining (Fig 11 A-H). Localization of platinum (II) complexes in perinuclear areas, nuclei and nucleoli was previously described, without further rationalization of their differential binding to specific subcellular compartments.[7d, 6f]

Conclusions

We report herein the synthesis, characterization and photophysical properties, supported by DFT/TD-DFT calculations of luminescent pentafluorophenyl cyclometalated platinum (II) [Pt(C^N-κ*C*,*N*)(HC^N-κ*N*)(C_6F_5)] **2** [obtained from the bis(HC^N)$_2$ complexes [Pt(HC^N-κ*N*)$_2$(C_6F_5)$_2$] **1**], and of solvate complexes [Pt(C^N)(C_6F_5)(DMSO)] (**3**). Upon irradiation, all complexes **1**-**3** exhibited in general long-lived emission in fluid degassed solutions or solid at 298 K and at 77 K. On basis on the emission spectra observed and theoretical calculations, the luminescence of complexes **1** has been assigned to metal to ligand charge transfer ^{3}ML'CT (Pt →HCN) excited state with some intraligand ^{3}IL' (HC^N) character and the emission of

cyclometalated complexes (**2** and **3**) to a mixed ^{3}IL/^{3}MLCT excited state with lower contribution of metal to ligand charge transfer in the solvate complexes **3**.

Solvate complexes **3a**, **3b** and **4** show three or four times less cytotoxicity toward the tumor A549 cell line than the cisplatin and double cytotoxicity for NL20 non-tumorigenic cells under the same experimental conditions. Fluorescent microscopy revealed efficient localization of complexes **3a**, **3b** and **4** on living A549, NL20 human cells and mouse embryonic fibroblasts (LMEFs) in the cytoplasm, with brighter emission in the perinuclear area, with subtle differences among them and between cell lines.

Experimental Section

General Comments. All reactions were carried out under an atmosphere of dry argon, using standard Schlenk techniques. Solvents were obtained from a solvent purification system (M-BRAUN MB SPS-800). Elemental analyses were carried out with a Carlo Erba EA1110 CHNS-O microanalyzer. Mass spectra were recorded on a Microflex MALDI-TOF Bruker (MALDI) spectrometer operating in the linear and reflector modes using dithranol as matrix or on a HP-5989B mass spectrometer (ES). IR spectra were obtained on a Nicolet Nexus FT-IR Spectrometer from Nujol mulls between polyethylene sheets. NMR spectra were recorded on a Bruker Avance 400 spectrometer at 298 K. Chemical shifts are reported in parts per million (ppm) relative to external standards ($SiMe_4$ for ^{1}H and $CFCl_3$ for $^{13}C\{^1H\}$), and all coupling constants are given in hertz (Hz). The NMR spectral assignments of the 2-(2'-thienyl)pyridine (Hthpy), 2-phenylbenzo[d]thiazole (Hbt) and 2-phenylquinoline (Hpq) ligands follow the numbering scheme shown in Scheme 1. The UV−vis absorption spectra were measured with a Hewlett-Packard 8453 spectrophotometer. Excitation and emission spectra were obtained in a Jobin Yvon Horiba Fluorolog 3-11, Tau 3 spectrofluorimeter. The lifetime measurements were performed with a Jobin Yvon Horiba Fluorolog operating in the phosphorimeter mode (with an F1-1029 lifetime emission PMT assembly, using a 450 W Xe lamp) or with a Datastation HUB-B with a nanoLED controller and software DAS6. The nanoLEDs employed for lifetime measurements were of 390, 370, 350 or 320 nm with pulse lengths of 0.8–1.4 ns. Quantum yields in solid or degassed solution were measured using a F-3018 Integrating Sphere mounted on a Fluorolog 3-11 Tau-3 spectrofluorimeter. The lifetime data have been fitted using the Jobin-Yvon software

package. The complexes [*cis*-Pt(C_6F_5)$_2$(THF)$_2$],[26] [*cis*-Pt(C_6F_5)$_2$(DMSO)$_2$],[27] 2-phenylbenzo[d]thiazole (Hbt)[28] and [Pt(C_6F_5)(ppy)(DMSO)][11b] were prepared as reported in the literature. 2-(2'-thienyl)pyridine (Hthpy) and 2-phenylquinoline (Hpq) were obtained from commercial supplies.

Preparation of [Pt(Hthpy-*κN*)$_2$(C_6F_5)$_2$] 1a. To a colourless solution of [*cis*-Pt(C_6F_5)$_2$(THF)$_2$] **(**0.250 g, 0.371 mmol) in CH_2Cl_2 (20 mL), 2-(2'-thienyl)pyridine (Hthpy) (0.120 g, 0.742 mmol) was added. After 2 h of stirring, the palid yellow solution obtained was evaporated to dryness and treated with *n*-hexane (5 mL) to afford **1a** as a white solid (0.278 g, 89 %) of orange luminescence. Slow crystallization from CH_2Cl_2/*n*-hexane at 298 K gives white crystals with yellow luminescence. Anal. Calcd for $C_{31}H_{16}F_{10}N_2PtS_2$: C, 43.01; H, 1.86; N, 3.24; S, 7.41. Found: C, 42.93; H, 1.95; N, 3.65; S, 7.01 %. MALDI-TOF (+): *m/z* (%) 683 [M-C_6F_5 + H]$^+$ (10); MALDI-TOF (-): *m/z* (%) 696 [Pt(C_6F_5)$_3$]$^-$ (20). IR (cm^{-1}): ν(C-F) 1060 (m), 952 (m); ν(C_6F_5)$_{X\text{-}sens}$ 805 (s), 796 (s). ^{1}H NMR (400.1 MHz, $CDCl_3$, δ): 8.50 (d, *J* = 3.2, 2H, H$^{11}_{thpy}$), 7.90 (d, *J* = 5.4, $^3J_{Pt\text{-}H}$ = 28.0, 2H, H$^2_{thpy}$), 7.54 (td, *J* = 7.9, *J* = 1.4, 2H, H$^4_{thpy}$), 7.38 (d, *J* = 6.9, 2H, H$^9_{thpy}$), 7.23 (d, *J* = 7.8, 2H, H$^5_{thpy}$), 7.12 (t, *J* = 4.3, 2H, H$^{10}_{thpy}$), 6.69 (t, *J* = 6.7, 2H, H$^3_{thpy}$). ^{13}C{^{1}H} NMR (100.6 MHz, $CDCl_3$, δ): 153.8 (s, C$^6_{thpy}$), 153.0 (s, C$^2_{thpy}$), 140.9 (s, C$^7_{thpy}$), 136.7 (s, C$^4_{thpy}$), 130.3 (s, C$^{11}_{thpy}$), 128.6 (s, C$^9_{thpy}$), 127.9 (s, C$^{10}_{thpy}$), 126.3 (s, C$^5_{thpy}$), 123.5 (s, C$^3_{thpy}$). ^{19}F (376.5 MHz, $CDCl_3$, δ): -118.9 (m, br, 2*o*-F), -119.3 (m, br, 2*o*-F), -162.5 (t, 2*p*-F), -164.7 (m, br, 4*m*-F). ^{19}F (376.5 MHz, $CDCl_3$, 228 K, δ) -118.8 (d, $^3J_{Pt\text{-}oF}$ = 462, 2*o*-F), -119.3 (d, $^3J_{Pt\text{-}oF}$ = 412, 2*o*-F), -162.0 (t, 2*p*-F), -164.1 (m, 2*m*-F), -164.3 (m, 2*m*-F).

Preparation of [Pt(Hbt-*κN*)$_2$(C_6F_5)$_2$] 1b. This compound was obtained as a white solid (0.252g, 90%) following a procedure similar to **1a**, using as starting precursors [*cis*-Pt(C_6F_5)$_2$(THF)$_2$] **(**0.200 g, 0.297 mmol) and 2-phenylbenzo[d]thiazole (Hbt) (0.125 g, 0.594 mmol). ESI(+): *m/z* (%) 952 [M]$^+$ (3). Anal. Calcd for $C_{38}H_{18}F_{10}N_2PtS_2$: C, 47.95; H, 1.91; N, 2.94; S, 6.74. Found: C, 47.65; H, 2.19; N, 3.19; S, 6.38 %. IR (cm^{-1}): ν(C-F) 1066 (m), 961 (m); ν(C_6F_5)$_{X\text{-}sens}$ 806 (s), 796 (s). ^{1}H NMR (400.1 MHz, $CDCl_3$, *δ*): 8.13 (d, *J* = 7.5, 4H, H^8, Ph), 7.84 (d, *J* = 8.1, 1H, H^7), 7.52 (d, *J* = 7.8, 2H, H^4), 7.23 (t, *J* = 7.2, 2H, H^5), 7.15 (t, *J* = 7.6, 2H, H^6), 7.03 (t, *J* = 7.5, 4H, H^9, Ph), 6.84 (t, *J* = 7.4, 2H, H^{10}). ^{13}C{^{1}H} NMR (100.6 MHz, $CDCl_3$, *δ*): 171.5 (s, C^2), 150.9 (s, C^{3a}), 132.0 (s,

C^{7a}), 131.6 (s, C^{13}), 130.2 (m, C^{10}), 128.6 (s, C^{9}, Ph), 127.5 (m, C^{8}, Ph), 125.9 (s, C^{6}), 125.7 (s, C^{5}), 124.6 (m, C^{7}), 120.7 (s, C^{4}). ^{19}F (376.5 MHz, $CDCl_3$, δ): -118.8 (d, $^3J_{Pt\text{-}oF}$ = 512, 2*o*-F), -121.3 (d, $^3J_{Pt\text{-}oF}$ = 390, 2*o*-F), -162.3 (t, 2*p*-F), -164.7 (m, 2*m*-F), -164.9 (m, 2*m*-F).

Preparation of [Pt(Hpq-*κN*)$_2$(C_6F_5)$_2$] 1c. This compound was obtained as a white solid (0.200g, 54%) with an orange emission, following a procedure similar to **1a**, using as starting materials [*cis*-Pt(C_6F_5)$_2$(THF)$_2$] (0.250 g, 0.397 mmol) and 2-phenylquinoline (Hpq) (0.163 g, 0.795 mmol). Slow crystallization from CH_2Cl_2/*n*-hexane at 298 K gives white crystals with yellow luminescence. ESI (+): *m/z* (%) 774 $[M\text{-}C_6F_5]^+$ (3). MALDI-TOF (-): *m/z* (%) 696 $[Pt(C_6F_5)_3]^-$ (30). Anal. Calcd for $C_{42}H_{22}F_{10}N_2Pt$: C, 53.68; H, 2.36; N, 3.98. Found: C, 53.44; H, 2.69; N, 3.68 %. IR (cm^{-1}): ν(C-F) 1064 (m), 957 (m); ν(C_6F_5)$_{X\text{-}sens}$ 803 (s), 791 (s). ^{1}H NMR (400.1 MHz, $CDCl_3$, *δ*): 8.62 (d, *J* = 8.7, 1H, H^8), 8.12 (d, *J* = 8.3, 1H, H^3), 7.57 (d, *J* = 7.8, 1H, H^5), 7.47 (m, br, 2H, $H^{9,9'}$), 7.30 (t, *J* = 7.0, 1H, $H^6{}_{pq}$), 7.19 (t, *J* = 7.7, 1H, $H^7{}_{pq}$), 7.12 (d, *J* = 8.3, 1H, $H^4{}_{pq}$), 6.81 (m, br, 2H, $H^{10,10'}$), 6.71 (t, *J* = 7.0, 1H, H^{11}). ^{1}H NMR (400.1 MHz, $CDCl_3$, 223K, *δ*): 8.68 (s, br, 1H, H^9), 8.48 (d, *J* = 8.9, 1H, H^8), 8.16 (d, *J* = 8.2, 1H, H^3), 7.59 (d, *J* = 7.9, 1H, H^5), 7.40 (t, *J* = 7.5, 1H, H^{10}), 7.31 (t, *J* = 7.2, 1H, H^6), 7.17 (t, *J* = 8.1, 1H, H^7), 7.12 (d, *J* = 8.2, 1H, H^4), 6.64 (t, *J* = 7.2, 1H, H^{11}), 6.17 (m, 2H, $H^{10',9'}$). ^{13}C{^{1}H} NMR (100.6 MHz, $CDCl_3$, *δ*): 163.7 (s, C^2), 146.8 (s, C^{4a}), 140.8 (s, C^{8a}), 138.1 (s, C^3), 131.3 (s, C^8), 129.3 (s, C^7), 128.4 (s, C^{11}), 127.8-127.4 (m, $C^{9,\,9',\,10,\,10',\,14}$), 126.8 (s, C^6), 126.7 (s, C^5), 125.1 (s, C^4). ^{19}F (376.5 MHz, $CDCl_3$, δ): -118.0 (d, $^3J_{Pt\text{-}oF}$ = 500, 2*o*-F), -121.6 (d, $^3J_{Pt\text{-}oF}$ = 389, 2*o*-F), -163.4 (t, 2*p*-F), -165.7 (m, 4*m*-F).

Preparation of [Pt(thpy-*κC,N*)(Hthpy-*kN*)(C_6F_5)] 2a. A white suspension of [Pt(Hthpy-*kN*)$_2$(C_6F_5)$_2$] (**1a**) (0.150 g, 0.176 mmol) in xylene (3 mL) was stirring at reflux during 2 hours. The orange solution obtained was evaporated to dryness and treated with *n*-hexane (5 mL) affording **2a** as an orange solid (0.084 g, 70%). MALDI-TOF(+): *m/z* (%) 516 $[M\text{-}C_6F_5]^+$ (31). Anal. Calcd for $C_{24}H_{13}F_5N_2PtS_2$: C, 42.17; H, 1.92; N, 4.10; S, 9.38. Found C, 42.53; H, 2.32; N, 4.35; S, 9.66 %. IR (cm^{-1}): ν(C-F) 1063 (m), 954 (m); ν(C_6F_5)$_{X\text{-}sens}$ 800 (vs). ^{1}H NMR (400.1 MHz, $CDCl_3$, *δ*): 9.19 (d, *J* = 5.5, $^3J_{Pt\text{-}H}$= 25, 1H, $H^{2'}$), 8.10 (d, *J* = 3.5, 1H, H^{11}), 7.87 (t, *J* = 7.5, 1H, $H^{4'}$), 7.77 (d, *J* = 7.9, 1H, $H^{5'}$), 7.70 (t, *J* = 7.7, 1H, H^4), 7.58 (d, *J* = 5.5, $^3J_{Pt\text{-}H}$ = 27, 1H, H^2), 7.42-7.40

(m, 2H, $H^{9,5}$), 7.32-7.28 (m, 2H, $H^{9',3'}$), 7.00 (t, J = 4.0, 1H, H^{10}), 6.80 (t, J = 6.3, 1H, H^{3}), 6.46 (d, J = 4.7, $^{3}J_{Pt\text{-}H}$ = 26, 1H, $H^{10'}$). $^{13}C\{^{1}H\}$ NMR (100.6 MHz, $CDCl_3$, δ): 161.6 (s, C^{6}), 154.8 (s, $C^{6'}$), 153.4 (d, J = 2.6, $^{2}J_{Pt\text{-}C}$ = 12, $C^{2'}$), 146.9 (s, $^{2}J_{Pt\text{-}C}$ = 12.4, C^{2}), 142.9 (s, $C^{11'}$), 140.2 (s, $C^{7'}$), 140.0 (s, C^{7}), 138.8 (s, C^{4}), 138.1 (s, $C^{4'}$), 135.2 (s, $C^{10'}$), 129.5 (s, C^{11}), 129.2 (s, $C^{9/5}$), 128.1 (s, $C^{3'/9'}$), 127.6 (s, C^{10}), 125.7 (s, $^{3}J_{Pt\text{-}C}$ = 11.2, $C^{5'}$), 123.2 (s, $C^{3'/9'}$), 119.9 (s, C^{3}), 117.8 (s, $C^{9/5}$). ^{19}F (376.5 MHz, $CDCl_3$, δ): -116.8 (dm, $^{3}J_{Pt\text{-}oF}$ = 455, 1*o*-F), -119.5 (dm, $^{3}J_{Pt\text{-}oF}$ = 495, 1*o*-F), -163.2 (t, 1*p*-F), -164.8 (m, 1*m*-F), -165.1 (m, 1*m*-F).

Preparation of [Pt(bt-$\kappa C,N$)(Hbt-κN)(C_6F_5)] 2b. This complex was prepared as a yellow solid (0.102 g, 60 %) in a similar way to **2a** starting from [Pt(Hbt-κN)$_2$(C_6F_5)$_2$] (**1b**) (0.200 g, 0.210 mmol). Anal. Calcd for $C_{32}H_{17}F_5N_2PtS_2$: C, 49.04; H, 2.19; N, 3.57; S, 8.18. Found: C, 49.33; H, 2.51; N, 3.97; S, 7.93 %. MALDI-TOF (-): *m/z* (%) 822 $[M+K]^+$ (33). IR (cm^{-1}): ν(C-F) 1060 (m), 957 (m); $\nu(C_6F_5)_{X\text{-}sens}$ 801 (m). ^{1}H NMR (400.1 MHz, $CDCl_3$, δ): 9.12 (m, 1H, $H^{7'}$), 8.43 (d, J = 7.6, 2H, H^{8}, Ph), 7.93 (m, 1H, $H^{4'}$), 7.84 (d, J = 8.0, 1H, H^{7}), 7.63 (d, J = 7.5, 1H, $H^{8'}$), 7.54 (t, J = 7.4, 1H, H^{10}), 7.48-7.45 (m, 2H, $H^{6',5'}$), 7.43 (t, J = 7.7, 2H, H^{9}, Ph), 7.22 (t, J = 7.6, 1H, H^{6}), 7.10 (t, J = 7.2, 1H, $H^{9'}$), 7.00 (t, J = 7.4, 1H, $H^{10'}$), 6.95 (t, J = 7.8, 1H, H^{5}), 6.75 (d, J = 7.6, $^{3}J_{Pt\text{-}H}$= 68, 1H, $H^{11'}$), 6.60 (d, J = 8.4, 1H, H^{4}). $^{13}C\{^{1}H\}$ NMR (100.6 MHz, $CDCl_3$, δ): 182.5 (s, $C^{2'}$), 172.1 (s, C^{2}), 153.3 (s, $C^{3a'}$), 150.67 (s, C^{7a}), 141.1 (s, $C^{12'}$), 139.5 (s, $C^{13'}$), 136.7 (s, $C^{11'}$), 132.3-132.0 (s, $C^{3a,\ 13,\ 10',\ 7a',\ 10}$), 129.02 (s, C^{9}, Ph), 128.6 (s, C^{8}, Ph), 127.4 (s, C^{5}), 127.1 (s, $C^{6'/5'}$), 126.7 (s, $C^{6'/5'}$), 125.7 (s, $C^{8'}$), 125.4 (s, $C^{7'}$), 125.0 (s, C^{6}), 123.8 (s, $C^{9'}$), 122.8 (s, C^{7}), 121.5 (s, $C^{4'}$), 118.6 (s, C^{4}). ^{19}F (376.5 MHz, $CDCl_3$, δ): -116.4 (dm, $^{3}J_{Pt\text{-}oF}$ = 496, 1*o*-F), -118.2 (dm, $^{3}J_{Pt\text{-}oF}$ = 500, 1*o*-F), -163.4 (t, 1*p*-F), -164.9 (m, 2*m*-F).

Preparation of [Pt(pq-κCN)(Hpq-κN)(C_6F_5)] 2c. This complex was prepared as an orange solid (0.077 g, 41 %) in a similar way to **2a** starting from [Pt(Hpq-κN)$_2$(C_6F_5)$_2$] (**1c**) (0.150 g, 0.238 mmol). Anal. Calcd for $C_{36}H_{21}F_5N_2Pt$: C, 56.03; H, 2.74; N, 3.63. Found: C, 56.41; H, 3.08; N, 3.97 %. MALDI-TOF (+): *m/z* (%) 604 $[M\text{-}C_6F_5]^+$ (89). IR (cm^{-1}): ν(C-F) 1059 (m), 958 (m); $\nu(C_6F_5)_{X\text{-}sens}$ 798 (s). ^{1}H NMR (400.1 MHz, $CDCl_3$, δ): 9.86 (d, J = 8.7, 1 H), 8.35 (d, J = 8.4, 1 H), 8.19 (d, J = 8.7, 1 H), 7.71-7.79 (m, 5 H), 7.69-7.64 (m, 3 H), 7.55-7.49 (m, 3 H), 7.21 (m,1 H), 7.09 (t, 3 H), 6.97 (t,1 H),

6.87-6.80 (m, 2 H). $^{13}C\{^{1}H\}$ NMR (100.6 MHz, $CDCl_3$, δ): 167.3 (s), 162.7 (s), 147.9 (s), 147.7 (s), 146.3 (s), 141.0 (s), 139.7 (s), 138.9 (s), 138.4 (s), 137.1 (s), 130.7 (s), 130.5 (s), 130.2 (s), 129.6 (s), 129.3 (s), 128.9 (s), 128.5-128.4 (m, 3 C), 128.0 (s), 127.9 (s), 127.7-127.6 (s, 3 C), 125.7 (s), 125.6 (s), 125.5 (s), 124.6 (s), 123.2 (s), 117.1 (s). ^{19}F (376.5 MHz, $CDCl_3$, δ): -116.8 (dm, $^{3}J_{Pt\text{-}oF}$ = 503, 1*o*-F), -118.0 (d, $^{3}J_{Pt\text{-}oF}$ = 461, 1*o*-F), -163.9 (t, 1*p*-F), -165.1 (m, 1*m*-F), -165.1 (m, 1*m*-F).

Preparation of [Pt(thpy-$\kappa C,N$)(C_6F_5)(DMSO)] 3a. To a white suspension of [*cis*-$Pt(C_6F_5)_2(DMSO)_2$] (0.181 g, 0.260 mmol) in xylene (5 mL), 2-(2'-thienyl)pyridine (Hthpy) (0.042 g, 0.260 mmol) was added. After 3h of stirring at reflux, the orange solution was cooled at 0º, obtaining **3a** as an orange solid (0.108 g, 70%). Anal. Calcd. for $C_{17}H_{12}F_5NOPtS_2$: C, 34.00; H, 2.01; N, 2.33; S, 10.68. Found: C, 34.33; H, 2.28; N, 2.70; S, 11.06 %. ESI (+): *m/z* (%) 523 $[M\text{-dmso}]^+$ (17), 601 $[M]^+$ (6). IR (cm^{-1}): ν(C-F) 1060 (m), 956 (m); $\nu(C_6F_5)_{X\text{-}sens}$ 801 (m). ^{1}H NMR (400.1 MHz, $CDCl_3$, δ): 9.46 (d, *J* = 5.6, $^{3}J_{Pt\text{-}H}$ = 28.4, 1H, $H^{2'}$), 7.81 (t, *J* = 7.5, 1H, $H^{4'}$), 7.43 (d, *J* = 7.8, 1H, $H^{5'}$), 7.23 (d, *J* = 4.7, 1H, $H^{9'}$), 7.13 (t, *J* = 6.4, 1H, $H^{3'}$), 6.04 (d, *J* = 4.7, $^{3}J_{Pt\text{-}H}$ = 27, 1H, $H^{10'}$), 3,07 (s, $^{3}J_{Pt\text{-}H}$ = 16, 6H, DMSO). $^{13}C\{^{1}H\}$ NMR (100.6 MHz, $CDCl_3$, δ): 161.2 (s, $^{2}J_{Pt\text{-}C}$ = 61, $C^{6'}$), 150.6 (s, $C^{2'}$), 149.9 (s, $^{1}J_{Pt\text{-}C}$ = 1002, $C^{11'}$), 144.4 (s, $^{2}J_{Pt\text{-}C}$ = 66.4, $C^{7'}$), 139.9 (s, $C^{4'}$), 133.7 (s, $^{2}J_{Pt\text{-}C}$ = 146, $C^{10'}$), 127.8 (s, $^{3}J_{Pt\text{-}C}$ = 81.4, $C^{9'}$), 121.1 (s, $^{3}J_{Pt\text{-}C}$ = 14.6 $C^{3'}$), 118.0 (s, $^{3}J_{Pt\text{-}C}$ = 26.1, $C^{5'}$), 45.2 (s, $^{2}J_{Pt\text{-}C}$ = 42.4, DMSO). ^{19}F (376.5 MHz, $CDCl_3$, δ): -116.9 (dm, $^{3}J_{Pt\text{-}oF}$ = 477, 2*o*-F), -159.2 (t, 1*p*-F), -161.9 (m, 2*m*-F).

Preparation of [Pt(bt-$\kappa C,N$)(C_6F_5)(DMSO)] 3b. A yellow suspension of [Pt(bt-$\kappa C,N$)(Hbt-κN)(C_6F_5)] (**2b**) (0.150 g, 0.192 mmol) in dimethyl sulfoxide (3 mL) was stirring at reflux during 4 hours. The orange solution was evaporated to dryness and treated with *n*-hexane (20 mL). In order to remove the Hbt generated in the reaction, the solvent was decanted and the white solid residue was treated with cold isopropanol (5 mL) obtaining **3b** (0.060g, 40%). Anal. Calcd for $C_{21}H_{14}F_5NOPtS_2$: C, 38.77; H, 2.17; N, 2.15; S, 9.86. Found: C, 38.40; H, 2.34; N, 2.41; S, 10.18 %. ESI (+): *m/z* (%) 651 $[M+H]^+$ (65), 484 $[M\text{-}C_6F_5]^+$ (50). IR (cm^{-1}): ν(C-F) 1066 (m), 957 (m); $\nu(C_6F_5)_{X\text{-}sens}$ 805 (m). ^{1}H NMR (400.1 MHz, $CDCl_3$, δ): 9.05 (d, *J* = 8.5, 1H, $H^{7'}$), 7.89 (d, *J* = 8.0, 1H, $H^{4'}$), 7.63 (d, *J* = 7.5, 1H, $H^{8'}$), 7.59 (t, *J* = 8.0, 1H, $H^{6'}$), 7.46 (t, *J* = 7.5, 1H, $H^{5'}$), 7.14 (t, *J* = 7.6, 1H, $H^{9'}$), 7.04 (t, *J* = 7.5, 1H, $H^{10'}$), 6.35 (d, *J* = 7.8, $^{3}J_{Pt\text{-}H}$ = 63, 1H,

H$^{11'}$), 3.04 (s, $^{3}J_{Pt\text{-}H}$ = 13, 6H, DMSO). ^{13}C{^{1}H} NMR (100.6 MHz, $CDCl_3$, δ): 183.5 (s, C$^{2'}$), 150.6 (s, C$^{3a'}$), 145.2 (s, C$^{13'}$), 141.7 (s, C$^{12'}$), 135.7 (s, C$^{11'}$), 131.8 (s, C$^{10'}$), 131.4 (s, C$^{7a'}$), 127.9 (s, C$^{6'}$), 126.1 (s, C$^{9'}$), 126.0 (s, C$^{5'}$), 125.8 (s, C$^{8'}$), 122.5 (s, C$^{4'}$), 121.7 (s, C$^{7'}$), 46.3 (s, $^{2}J_{Pt\text{-}C}$ = 40.0, DMSO). ^{19}F (376.5 MHz, $CDCl_3$, δ): -116.9 (dm, $^{3}J_{Pt\text{-}oF}$ = 503, 2*o*-F), -159.0 (t, 1*p*-F), -161.4 (m, 2*m*-F).

X-ray Crystallography. Details of the X-ray analyses are summarized in Table S5†. Yellow (**1a**, **1c** and **3b**) and orange (**2b** and **3a**) crystals were obtained by slow diffusion of *n*-hexane into solutions of the complexes in CH_2Cl_2 (**1a**, **1c**, **3a** and **3b**; -30ºC) or $CHCl_3$ (**2b**; room temperature), respectively. X-ray intensity data were collected with a NONIUS-κCCD area-detector diffractometer, using graphite-monochromatic Mo-K_α radiation, and images processed using the DENZO and SCALEPACK suite of programs,[29] carrying out the absorption correction at this point for complex **1a**. For the rest of the structures, the absorption correction was performed using MULTI-SCAN[30] (**1c**, **2b** and **3a**) or XABS2[31] (**3b**), with the WINGX program suite.[32] The structures were solved by Patterson and Fourier methods using DIRDIF2008[33] (**1a**) and SIR-2004[34] (**1c**, **2b** and **3a**) or by intrinsic phasing using SHELXT (**3b**),[35] and refined by full-matrix least squares on F^2 with SHELXL.[36] All non-hydrogen atoms were assigned anisotropic displacement parameters. All the hydrogen atoms were constrained to idealized geometries fixing isotropic displacement parameters 1.2 times the U_{iso} value of their attached carbon for the aromatic carbons and 1.5 times for the methyl groups. For **1a**, positional disorder (70/30) was observed with respect to the position of the sulphur atom in the thienyl rings of both of the pyridine ligands. For **1c**, disordered crystallization molecules of CH_2Cl_2 were observed, but could not be properly modelled. Examination with PLATON[37] and SQUEEZE[37-38] revealed the presence of two voids of 160 Å^3 in the unit cell, containing each of them 73 e$^-$, which fits well with the presence of 3 molecules of CH_2Cl_2 in the unit cell (**1c**·0.75CH_2Cl_2). Finally, the structures show some residual peaks greater than 1 eA^{-3}, but with no chemical meaning.

Computational details

Calculations of all complex were carried out with the Gaussian 09 package[39] using Becke's three-parameter functional combined with Lee−Yang−Parr's correlation

functional (B3LYP) in the singlet state (S_0) and the unrestricted U-B3LYP in the triplet state (T_1).[40] Optimizations on the singlet state (S_0) were performed using as a starting point the molecular geometry obtained through X-ray diffraction analysis. No negative frequency was found in the vibrational frequency analysis of the final equilibrium geometries. The basis set used was the LanL2DZ effective core potential for the Pt and 6-31G(d,p) for the ligand atoms.[41] DFT, UDFT and TD-DFT calculations were carried out using the polarized continuum model approach[42] implemented in the Gaussian 09 software. Overlap populations between molecular fragments were calculated using the GaussSum program.[43]

Cell culture

Human lung cell lines A549 (adenocarcinomic alveolar basal epithelial cells) and NL20 (immortalized bronchial epithelial cells), and immortalized mouse embryonic fibroblasts (3T3) obtained from lungs (LMEFs), were cultured following the American Type Culture Collection (www.atcc.org) recommendations and standard methods. A549 and LMEFs cells were maintained in RPMI 1640 and DMEM (Dulbecco's Modified Eagle's Medium) respectively, supplemented with 10% fetal bovine serum (FBS) and 2.0 mM L-glutamine. NL20 cell line was grown in Ham's F-12 medium supplemented with 1.5 g/L sodium bicarbonate, 2.7 g/L glucose, 2.0 mM L-glutamine, 0.1 mM non-essential aminoacids, 0.005 mg/mL insulin, 10 ng/mL epidermal growth factor, 0.001 mg/mL transferrin, 500 ng/mL hydrocortisone and 4% FBS. Penicillin (100 U/mL) and streptomycin (100 μg/mL) was added to all media. Cultures were maintained under a humidified atmosphere of 95% air/5% CO2 at 37 °C, and were sub-cultured before they get confluent using a 0.25% trypsin-EDTA solution.

Cytotoxicity assay

The MTS (3-(4,5-dimethylthiazol-2-yl)-5-(3-carboxymethoxyphenyl)-2-(4-sulfophenyl)-2H-tetrazolium) hydrolysis method (MTS-based CellTiter® 96. AQueous Assay; Promega Corp., Madison, WI) was used to determine the cell viability as an indicator for A549 and NL20 cells sensitivity to the complexes. 50 μL of exponentially growing cells were seeded at a density of $1.5x10^3$ (A549) or $7.0x10^3$ (NL20) cells per well, in a 96-well flat-bottomed microplate in their respective cell culture growing media with reduced concentrations of FBS, 5% in case of A549 and 2% for NL20. 24 h

later they were incubated for 72 h with the compounds. The complexes were dissolved at their maximal solubility in DMSO (**3a** and **4** at 16 mM, and **3b** at 8 mM) and cisplatin (Alfa Aesar; Karlsruhe, Germany), as a reference, was dissolved at 6.4 mM in saline solution (0.15 M NaCl).[44] These stock solutions were kept frozen until they were dissolved in test medium as nine 2X serial dilutions (1:1.5). 50 µL of each compound dilution or medium alone was added to growing cells in the 96-well plate designed as previously recommended.[45] Final concentrations in sextuplicates ranged from: 3.12 to 80 µM (**3a**, **3b** and **4)**, and 1.56 to 40 µM (cisplatin) for A549 cells; 3.12 to 80 µM (**3a** and **4)**, 1.38 to 35.5 µM (**3b**) and 0.69 to 17.77 µM (cisplatin) for NL20 cells. After 72 h at 37 °C, 20 µl of MTS was added and plates were incubated for 1–2 h at 37 °C. Finally, the optical density was measured at 590 nm using a 96-well multiscanner autoreader (POLARstar Omega, BMG Labtech; Germany). Each experiment was repeated three times. Appropriate solvent controls were run along with samples to discard DMSO cytotoxic effect at concentrations ≤1%. The IC_{50} (drug concentration that produced 50% inhibition of cell proliferation) was calculated by plotting percentage of growing inhibition *versus* log of the drug concentration using the GraphPad Prism 6 (La Jolla, CA) software.

Localization in cells

A549 and NL20 cells were cultured over one cm diameter Poly-L-Lysine coated coverslips into a 24-well plate with 1 mL/well of supplemented culture medium for 48 h. After incubation at 37ºC for 30 min in 1 mL of a new cell line specific medium containing 40 µM of each compound and 3.2 µM of Hoechts 33258 (Sigma), the cells were finally washed twice in phosphate buffer saline (PBS, pH 7.2). Hoechts 33258 was added as a fluorescent stain for chromosomes suitable for nuclei staining in living cells due to its non toxic effect and permeability through cell membranes.[24] As control to discard emission bleeding between light channels, the incubation of cells was also performed separately with each compound (**3a, 3b** and **4**) and also with Hoechts alone. Cells were finally washed twice in phosphate buffer saline (PBS, pH 7.2). Coverslips were removed, mounted on glass slides and sealed with vaseline before been immediately examined under a fluorescence microscope (Leica DM600B). The microscope was equipped with a Nomarski differential interference contrast for transmitted light, and with an incident light fluorescence illuminator accommodating three filter cubes (N2.1: λ_{ex} filter BP 515-60, dichromatic mirror 580, suppression filter

λ_{em} LP 590; Y5: λ_{ex} filter BP 620/60, dichromatic mirror 660, suppression filter λ_{em} BP 700/75; and A4: λ_{ex} filter BP 360/40, dichromatic mirror 400, suppression filter λ_{em} BP 470/40) (Leica), suitable for imaging switching between Nomarski DIC transmitted light, and green, red and blue fluorescent light channels. Images were documented using a 100X objective (Leica PLAN APO) and a B&W digital camera (Hamamatsu ORCA R2, mod. C10600) with a help of Micro-Manager Open Source Microscopy Software and Fiji/ImageJ free software.[46]

†Electronic Supplementary Information (ESI). CCDC 1412694-1412698. NMR spectra, crystallographic, photophysical, theoretical data, figures of UV-vis in cellular medium, cytotoxicity and cell fluorescence images for compounds prepared in this paper. For ESI and crystallographic data in CIF or other electronic format see DOI: _____/_____

Acknowledgments. This work was supported by the Spanish MINECO (Project CTQ2013-45518-P) and by Fundación Rioja Salud (Gobierno de La Rioja, Spain) to J.G.P. The authors thank CESGA for computer support, M. Vilariño (CIBIR, Spain) for providing NL-20 cell line and advise with MTS assays, and J. Cabello (CIBIR, Spain) for help with fluorescent microscopy. S.P.-H. thanks the Sistema Riojano de Innovación (Gobierno de La Rioja, Spain) for a pHD grant.

References

1. N. J. Wheate, S. Walker, G. E. Craig and R. Oun, *Dalton Trans.*, 2010, **39**, 8113-8127.
2. (a) R. Y. Tsang, T. Al-Fayea and H. J. Au, *Drug-Safety*, 2009, **32**, 1109-1122; (b) M. J. Sullivan, *Cancer* 2009, **115**, 5623-5626; (c) B. Köberle, M. T. Tomicic, S. Usanova and B. Kaina, *BBA Rev. Cancer*, 2010, **1806**, 172-182; (d) C. Meijer, N. H. Mulder, H. Timmer-Bosscha, W. J. Sluiter, G. J. Meersma and E. G. E. de Vries, *Cancer Res.*, 1992, **52**, 6885-6889.
3. (a) N. Cutillas, G. S. Yellol, C. de Haro, C. Vicente, V. Rodríguez and J. Ruiz, *Coord. Chem. Rev.*, 2013, **257**, 2784-2797; (b) I. Omae, *Coord. Chem. Rev.*, 2014, **280**, 84-95.

4. (a) H.-K. Liu and P. J. Sadler, *Acc. Chem. Res.*, 2011, **44**, 349-359; (b) J. Suryadi and U. Bierbach, *Chem. Eur. J.*, 2012, **18**, 12926-12934; (c) J. Ruiz, C. Vicente, C. de Haro and A. Espinosa, *Inorg. Chem.*, 2011, **50**, 2151-2158; (d) T. Zou, J. Liu, C. T. Lum, C. Ma, R. C.-T. Chan, C.-N. Lok, W.-M. Kwok and C.-M. Che, *Angew. Chem., Int. Ed.*, 2014, **53**, 10119-10123.
5. J. Reedijk, *Platinum Met. Rev.*, 2008, **52**, 2-11.
6. (a) J. Kalinowski, V. Fattori, M. Cocchi and J. A. G. Williams, *Coord. Chem. Rev.*, 2011, **255**, 2401-2425; (b) J. A. G. Williams, in *Topics in Current Chemistry, Photochemistry and Photophysics of Coordination Compounds: Platinum*, Springer, Heidelberg, 2007, vol. 281; (c) J. A. G. Williams, S. Develay, D. L. Rochester and L. Murphy, *Coord. Chem. Rev.*, 2008, **252**, 2596-2611; (d) L. Murphy and J. A. G. Williams, *Top. Organomet. Chem.*, 2010, **28**, 75-111; (e) Y. Chi and P. T. Chou, *Chem. Soc. Rev.*, 2010, **39**, 638-655.
7. (a) M. Mauro, A. Aliprandi, D. Septiadi, N. S. Kehr and L. De Cola, *Chem. Soc. Rev.*, 2014, **43**, 4144-4166; (b) F. L. Thorp-Greenwood, *Organometallics*, 2012, **31**, 5686-5692; (c) Q. Zhao, C. Huang and F. Li, *Chem. Soc. Rev.*, 2011, **40**, 2508-2524; (d) E. Baggaley, J. A. Weinstein and J. A. G. Williams, *Coord. Chem. Rev.*, 2012, **256**, 1762-1785; (e) K. K.-W. Lo, A. W.-T. Choi and W. H.-T. Law, *Dalton Trans.*, 2012, **41**, 6021-6047; (f) R. W.-Y. Sun, A. L.-F. Chow, X.-H. Li, J. J. Yan, S. Sin-Yin Chui and C.-M. Che, *Chem. Sci.*, 2011, **2**, 728-736; (g) E. Baggaley, S. W. Botchway, J. W. Haycock, H. Morris, I. V. Sazanovich, J. A. G. Williams and J. A. Weinstein, *Chem. Sci.*, 2014, **5**, 879-886; (h) C. K. Koo, L. K. Y. So, K. L. Wong, Y. M. Ho, Y. W. Lam, M. H. W. Lam, K. W. Cheah, C. C. W. Cheng and W. M. Kwok, *Chem. Eur. J.*, 2010, **16**, 3942-3950.
8. (a) A. Colombo, F. Fiorini, D. Septiadi, C. Dragonetti, F. Nisic, A. Valore, D. Roberto, M. Mauro and L. De Cola, *Dalton Trans.*, 2015, **44**, 8478-8487; (b) W. A. Tarran, G. R. Freeman, L. Murphy, A. M. Benham, R. Kataky and J. A. G. Williams, *Inorg. Chem.*, 2014, **53**, 5738-5749.
9. S. Liu, H. Sun, Y. Ma, S. Ye, X. Liu, X. Zhou, X. Mou, L. Wang, Q. Zhao and W. Huang, *J. Mat. Chem.*, 2012, **22**, 22167-22173.
10. (a) J. R. Berenguer, E. Lalinde, M. T. Moreno, S. Sánchez and J. Torroba, *Inorg. Chem.*, 2012, **51**, 11665-11679; (b) J. Forniés, S. Ibáñez, E. Lalinde, A. Martín, M. T. Moreno and A. C. Tsipis, *Dalton Trans.*, 2012, 3439-3451; (c) M. Baya, Ú. Belío, J. Forniés, A. Martín, M. Perálvarez and V. Sicilia, *Inorg. Chim. Acta*,

2015, **424**, 136-149; (d) A. Martín, Ú. Belío, S. Fuertes and V. Sicilia, *Eur. J. Inorg. Chem.*, 2013, **2013**, 2231-2247; (e) J. Forniés, S. Ibáñez, A. Martín, M. Sanz, J. R. Berenguer, E. Lalinde and J. Torroba, *Organometallics*, 2006, **25**, 4331-4340; (f) J. Forniés, S. Ibáñez, A. Martín, B. Gil, E. Lalinde and M. T. Moreno, *Organometallics*, 2004, **23**, 3963-3975.

11. (a) J. R. Berenguer, E. Lalinde, A. Martín, M. T. Moreno, S. Ruiz, S. Sánchez and H. R. Shahsavari, *Chem. Commun.*, 2013, **49**, 5067-5069; (b) J. R. Berenguer, E. Lalinde, A. Martín, M. T. Moreno, S. Ruiz, S. Sánchez and H. R. Shahsavari, *Inorg. Chem.*, 2014, **53**, 8770-8785.
12. R. G. Pearson, *J. Am. Chem. Soc.*, 1963, **85**, 3533-3539.
13. J. R. Berenguer, J. Fernández, N. Giménez, E. Lalinde, M. T. Moreno and S. Sánchez, *Organometallics*, 2013, **32**, 3943-3953.
14. A. Bondi, *J. Phys. Chem.*, 1964, **68**, 441.
15. (a) M. Baya, Ú. Belío and A. Martín, *Inorg. Chem.*, 2013, **53**, 189-200; (b) E. Lalinde, M. T. Moreno, S. Ruiz and S. Sánchez, *Organometallics*, 2014, **33**, 3078-3090.
16. (a) M. M. Mdleleni, J. S. Bridgewater, R. J. Watts and P. C. Ford, *Inorg. Chem.*, 1995, **34**, 2334-2342; (b) S. Stoccoro, M. A. Cinellu, A. Zucca, G. Minghetti and F. Demartin, *Inorg.Chim. Acta*, 1994, **215**, 17-26; (c) J.-Y. Cho, K. Y. Suponitsky, J. Li, T. V. Timofeeva, S. Barlow and S. R. Marder, *J. Organomet. Chem.*, 2005, **690**, 4090-4093; (d) H. Fukuda, Y. Yamada, D. Hashizume, T. Takayama and M. Watabe, *Appl. Organomet. Chem.*, 2009, **23**, 154-160; (e) S. W. Lai, M. C. W. Chan, K. K. Cheung, S. M. Peng and C. M. Che, *Organometallics*, 1999, **18**, 3991-3997.
17. M. Calligaris, *Coord. Chem. Rev.*, 2004, **248**, 351-375.
18. V. Khlebnikov, M. Heckenroth, H. Muller-Bunz and M. Albrecht, *Dalton Trans.*, 2013, **42**, 4197-4207.
19. (a) J. Brooks, Y. Babayan, S. Lamansky, P. I. Djorovich, I. Tsyba, R. Bau and M. E. Thompson, *Inorg. Chem.*, 2002, **41**, 3055-3066; (b) J. Forniés, N. Giménez, S. Ibáñez, E. Lalinde, A. Martín and M. T. Moreno, *Inorg. Chem.*, 2015, **54**, 4351-4363.
20. (a) M. P. Barr, S. G. Gray, A. C. Hoffmann, R. A. Hilger, J. Thomale, J. D. O'Flaherty, D. A. Fennell, D. Richard, J. J. O'Leary and K. J. O'Byrne, *PLoS One* 2013, **8**, e54193; (b) B. D. Lopez-Ayllon, V. Moncho-Amor, A. Abarrategi, I. I.

de Cáceres, J. Castro-Carpeño, C. Belda-Iniesta, R. Perona and L. Sastre, *Cancer Med.*, 2014, **3**, 1099-1111.

21. (a) L. M. Levasseur, H. K. Slocum, Y. M. Rustum and W. R. Greco, *Cancer Res.*, 1998, **58**, 5749-5761; (b) S. B. Hassan, E. Jonsson, R. Larsson and M. O. Karlsson, *J. Pharmac. Exp. Ther.*, 2001, **299**, 1140-1147.
22. We would like to note that for complex **3a** in DMSO solution, the HE fluorecence band (located at 435 nm) is very weak (See Figure S24†). Therefore, no cross talk between the phosphorescent emission of the complex **3a** and the fluorophore (Hoechst 33258, λ_{em} 461 nm), was expected.
23. (a) R. W.-Y. Sun, C. K.-L. Li, D.-L. Ma, J. J. Yan, C.-N. Lok, C.-H. Leung, N. Zhu and C.-M. Che, *Chem. Eur. J.*, 2010, **16**, 3097-3113; (b) L.-K. Sy, S.-C. Yan, C.-N. Lok, R. Y. K. Man and C.-M. Che, *Cancer Res.*, 2008, **68**, 10229-10237.
24. R. M. Martin, H. Leonhardt and M. C. Cardoso, *Cytometry Part A*, 2005, **67A**, 45-52.
25. (a) S. W. M. Tanley, A. M. M. Schreurs, L. M. J. Kroon-Batenburg, J. Meredith, R. Prendergast, D. Walsh, P. Bryant, C. Levy and J. R. Helliwell, *Acta Crystallogr Section D Biol Crystallogr.*, 2012, **68**, 601-612; (b) P. M. Uribe, M. A. Mueller, J. S. Gleichman, M. D. Kramer, Q. Wang, M. Sibrian-Vazquez, R. M. Strongin, P. S. Steyger, D. A. Cotanche and J. I. Matsui, *PLoS ONE*, 2013, **8**, e55359.
26. R. Usón, J. Forniés, M. Tomás and B. Menjón, *Organometallics*, 1985, **4**, 1912-1914.
27. T. Yagyu, J.-i. Ohashi and M. Maeda, *Organometallics*, 2007, **26**, 2383-2391.
28. W. Bai, *J. Lumin.*, 2012, **132**, 2847-2854.
29. Z. Otwinowski and W. Minor, in *Methods in Enzymology*, eds. C. V. Carter, Jr. and R. M. Sweet, Academic Press, New York, 1997, vol. 276A, p. 307.
30. R. H. Blessing, *Acta Crystallogr.*, 1995, **A51**, 33-38.
31. I. P. Parkin, A. M. Z. Slawin, D. J. Williams and J. D. Woollins, *Inorg. Chim. Acta*, 1990, **172**, 159-163.
32. L. J. Farrugia, *Appl. Crystallogr.*, 1999, **32**, 837-838.
33. P. T. Beursken, G. Beursken, R. de Gelder, J. M. M. Smits, S. García-Granda and R. O. Gould, *DIRDIF2008.*, Crystallography Laboratory, Radboud University Nijmegen, Toernooiveld 1, 65525 ED Nijmegen, The Netherlands, 2008.

34. M. C. Burla, R. Caliandro, M. Camalli, B. Carrozzini, G. L. Cascarano, L. De Caro, C. Giacovazzo, G. Polidori and R. Spagna, *J. Appl. Crystallogr.*, 2005, **38**, 381-388.
35. G. M. Sheldrick, *Acta Crystallogr., Sect. A: Found. Crystallogr.*, 2015, **71**, 3-8.
36. G. M. Sheldrick, *Acta Crystallogr., Sect. C*, 2015, **71**, 3-8.
37. A. L. Speck, *J. Appl. Cryst.*, 2003, **36**, 7-13.
38. (a) A. L. Speck, *Acta Crystallogr., Sect C*, 2015, **71**, 9-18; (b) A. L. Speck, *Acta Crystallogr.*, 1990, **A46**, C.
39. M. J. Frisch, et al. Gaussian 09, Revision E.01:Gaussian, Inc., Wallingford, CT, 2009 (see the Supporting Information for the complete citation).
40. (a) A. D. Becke, *Phys. Rev. A*, 1988, **38**, 3098-3100; (b) A. D. Becke, *J. Chem. Phys.*, 1993, **98**, 5648-5652; (c) C. Lee, W. Yang and R. G. Parr, *Phys. Rev.*, 1988, **B37**, 785-789.
41. W. R. Wadt and P. J. Hay, *J. Chem. Phys.*, 1985, **82**, 284-298.
42. V. Barone and M. Cossi, *J. Phys. Chem. A*, 1998, **102**, 1995-2001.
43. N. M. O'Boyle, A. L. Tenderholt and K. M. Langner, *J. Comput. Chem.*, 2008, **29**, 839-845.
44. M. D. Hall, K. A. Telma, K.-E. Chang, T. D. Lee, J. P. Madigan, J. R. Lloyd, I. S. Goldlust, J. D. Hoeschele and M. M. Gottesman, *Cancer Res.*, 2014, **74**, 3913-3922.
45. OECD. 2010. Guidance Document on using Cytotoxicity Tests to Estimate Starting Doses for Acute Oral Systemic Toxicity Tests. No. 129, París, France. Available at: [http://www.oecd.org/env/testguidelines].
46. (a) A. Edelstein, N. Amodaj, K. Hoover, R. Vale and N. Stuurman, in *Computer Control of Microscopes Using μManager In Current Protocols in Molecular Biology*, John Wiley & Sons, Inc., 2001; (b) J. Schindelin, I. Arganda-Carreras, E. Frise, V. Kaynig, M. Longair, T. Pietzsch, S. Preibisch, C. Rueden, S. Saalfeld, B. Schmid, J.-Y. Tinevez, D. J. White, V. Hartenstein, K. Eliceiri, P. Tomancak and A. Cardona, *Nat Meth*, 2012, **9**, 676-682.

Table 1 Selected distances (Å) and angles (°) for complexes **1a**, **1c**·0.75CH_2Cl_2, **2b**, **3a** and **3b**

1a			
Distances (Å)		**Angles (°)**	
Pt-N(1)	2.110(3)	N(2)-Pt-N(1)	88.97(12)
Pt-N(2)	2.111(3)	N(2)-Pt-C(19)	88.80(14)
Pt-C(19)	2.012(4)	N(1)-Pt-C(25)	89.79(14)
Pt-C(25)	2.015(4)	C(25)-Pt-C(19)	92.46(16)
C(14)-C(15)	1.464(6)		
1c.0.75CH_2Cl_2			
Distances (Å)		**Angles (°)**	
Pt-N(1)	2.173(6)	N(2)-Pt-N(1)	90.1(2)
Pt-N(2)	2.133(5)	C(31)-Pt-N(2)	91.5(2)
Pt-C(31)	2.012(8)	C(31)-Pt-C(37)	87.2(3)
Pt-C(37)	2.011(6)	C(37)-Pt-N(1)	91.4(2)
2b			
Distances (Å)		**Angles (°)**	
Pt-N(1)	2.101(3)	N(2)-Pt-N(2)	96.90(12)
Pt-N(2)	2.152(3)	C(9)-Pt-N(1)	81.37(15)
Pt-C(9)	2.007(3)	C(27)-Pt-C(9)	91.20(15)
Pt-C(27)	2.005(4)	C(27)-Pt-N(2)	90.65(12)
Pt-H(22)	2.587		
Pt-H(15)	2.786		
3a			
Distances (Å)		**Angles (°)**	
Pt-N(1)	2.009(7)	C(10)-Pt(1)-C(1)	91.5(4)
Pt-C(1)	2.049(9)	C(1)-Pt(1)-N(1)	79.0(3)
Pt-S(2)	2.296(2)	C(10)-Pt(1)-S(2)	92.0(3)
Pt-C(10)	2.007(10)	N(1)-Pt-S(2)	98.09(18)
O(1)-S(2)	1.472(6)	O(1)-S(2)-Pt(1)	116.9(3)
S(2)-C(16)	1.789(9)		
S(2)-C(17)	1.795(9)		
3b			
Distances (Å)		**Angles (°)**	
Pt-N(1)	2.136(4)	C(14)-Pt(1)-C(9)	89.3(2)
Pt-C(9)	2.041(6)	C(9)-Pt(1)-N(1)	80.1(2)
Pt-C(14)	2.012(5)	C(14)-Pt(1)-S(2)	90.37(15)
Pt-S(2)	2.3140(13)	N(1)-Pt-S(2)	100.14(12)
S(2)-C(20)	1.775(5)	O(1)-S(2)-Pt(1)	118.23(15)
S(2)-C(21)	1.781(6)	O(1)-S(2)-C(20)	105.3(3)
O(1)-S(2)	1.475(4)	O(1)-S(2)-C(21)	109.4(3)
		C(20)-S(2)-C(21)	98.1(3)

Table 2 Absorption data for compounds **1**–**3** in CH_2Cl_2 and MeCN (5×10^{-5} M Solutions)

Compound	λ_{abs}/nm (10^3 ε/M^{-1} cm^{-1})
[Pt(Hthpy-κ*N*)$_2$(C_6F_5)$_2$] **1a**	230 (22.6), 262 (18.7), 284$_{sh}$ (19.9), 302 (23.0), 340$_{sh}$ (3.7) (CH_2Cl_2) 208 (18), 240 (13.6), 260 (12.5), 300 (15.9), 340 (1.6) (MeCN)
[Pt(Hbt-κ*N*)$_2$(C_6F_5)$_2$] **1b**	231 (47.1), 248 (41.1), 292 (27.9) (CH_2Cl_2)[a)] 227, 248, 254, 292 (MeCN)
[Pt(pq-κ*N*)$_2$(C_6F_5)$_2$] **1c**	258 (45.6), 295 (13.5), 322 (13.9), 338 (9.7) (CH_2Cl_2) 205 (69), 219 (53.5), 236 (45.3), 253 (52.0), 309 (5.1), 322 (7.1), 336 (1.4) (MeCN)
[Pt(thpy-κ*C*,*N*)(Hthpy-*kN*)(C_6F_5)] **2a**	228 (21.2), 255 (22.1), 279$_{sh}$ (20.4), 302 (26.2), 330 (11.2), 392 (5.6), 410 (4.7) (CH_2Cl_2) 220 (14.7), 248 (18.4), 274 (17.8), 298 (23.6), 328$_{sh}$ (9.2), 390 (3.3), 410 (2.8) (MeCN)
[Pt(bt-κ*C*,*N*)(Hbt-κN)(C_6F_5)$_2$] **2b**	230 (49.6), 257 (35.0), 270 (35.2), 309 (31.2), 320 (30.5), 335 (19.8), 366 (8.1), 397 (6.4), 420 (4.9) (CH_2Cl_2) 210 (49.5), 232$_{sh}$ (30.5), 251 (20.2), 267 (23.1), 276 (21.5), 308 (20.0), 326$_{sh}$ (15.1), 358 (3.8), 390 (2.7), 413 (1.9) (MeCN)
[Pt(pq-κ*C*,*N*)(Hpq-κ*N*)(C_6F_5)$_2$] **2c**	237 (35), 287 (18.6), 330 (9.1), 355 (7.2), 430 (2.7) (CH_2Cl_2) 213 (48.8), 255 (53.5), 274 (26.7), 285 (25.3), 322 (10.6), 336 (10.6), 349 (8.0), 418 (1.9) (MeCN)
[Pt(thpy-κ*C*,*N*)(C_6F_5)(DMSO)] **3a**	231 (38.9), 240$_{sh}$ (36.0), 260 (18.3), 288 (16.3), 300 (15.0), 318 (11.7), 381 (6.1), 398 (4.5) (CH_2Cl_2) 215 (20.1), 245 (19.53), 274 (13.0), 295 (15.7), 305 (15.1), 325 (12.2), 393 (5.5), 410 (4.7) (MeCN)
[Pt(bt-κ*C*,*N*)(C_6F_5)(DMSO)] **3b**	231 (24), 261 (20.5), 268$_{sh}$ (19.7), 319 (15.4), 332 (15.5), 370 (5.7), 390$_{sh}$ (4.2), 430 (0.8) (CH_2Cl_2) 220 (27.3), 254 (15.9), 265 (18.2), 316 (11.5), 330 (11.3), 358 (4.6), 390 (3.5), 410 (2.7) (MeCN)

[a)] Tail to 350 nm

Table 3 Photophysical data for complexes **1-4** in solid state and in CH_2Cl_2 degassed solution (5×10^{-5} M)

Complex	medium	298K					77K	
		λ_{em}/nm	ϕ/%	τ/μs	k_r[a]/s^{-1}	K_{nr}[b]/s^{-1}	λ_{em}/nm	τ/μs
1a	solid[c]	565, 605	12.2	20.0	6.1×10^3	4.4×10^4	520, 555, 600	83 (75%), 294 (25%)
	CH_2Cl_2[d]	490, 520, 560_{sh}	1.2	0.9	1.3×10^4	1.1×10^6	506, 550, 600_{sh}	234.3 (39%), 29.9 (41%)
1b	solid	516	14	102.8	1.4×10^3	8.4×10^3	480, 510	203.9 (510)
	CH_2Cl_2[d]	370, 540[e]	1.6 (370) 1.4 (540)	0.12 (53%), 0.02 (47%) (370) 2 (540)	2.2×10^5 7×10^3	1.3×10^7 4.9×10^5	475, 515, 560	7.5
1c	solid[c]	560, 595	3.6	12.8	4.9×10^3	7.3×10^4	560, 600	33.2 (76%), 538 (24%)
	CH_2Cl_2 [10^{-4} M]	485, 518, 560_{sh} [485, 550, 580]	3.7	0.6 (32%), 3.3 (68%)	1.5×10^4	4.0×10^5	475, 510, 550, 600_{sh} [485, 520, 560]	184 (72%), 773 (28%)
2a	solid	550, 570, 600, 620_{sh}, 650_{sh}	5.1	15.3 (550); 16.3 (600)	3.3×10^3	6.2×10^4	548, 560, 580, 600, 650_{sh}	16.9
	CH_2Cl_2[d]	555, 575, 600, 630_{sh}	1	0.9	1.1×10^4	1.1×10^6	550, 570, 595, 620_{sh}, 650_{sh}	31
2b	solid	530, 570, 620	16.5	12.4 (530); 10.8 (570)	1.5×10^4	7.7×10^4	525, 540, 570, 620	10.3 (525); 18.0 (570)
	CH_2Cl_2[d]	530, 570, 615_{sh}	4.4	1.1	4×10^4	8.7×10^5	515, 560, 600, 675_{sh}	18
2c	solid	550, 580, 625	1.1	9.2 (580)	1.2×10^4	1.1×10^5	555, 600	14.9
	CH_2Cl_2[d]	550, 580	9.7	1.1	8.8×10^4	8.2×10^5	548, 590	20.4
3a	solid	[f]					595, 615, 650	64.1
	CH_2Cl_2[d]	435, 550, 595	0.7 (435) 1.3 (550)	5.2×10^{-3} (59%), 0.11 (41%) (435); 8.5 (550)	1.5×10^5 1.5×10^3	2.1×10^7 1.2×10^5	545, 590	8.5
3b	solid	538, 580, 630_{sh}	2.5	12.4	2.0×10^3	7.9×10^4	545, 580, 630	26.0
	CH_2Cl_2[d]	530, 570, 610_{sh}	2.9	1.1	2.6×10^4	8.8×10^5	525, 570, 610	19.4
4[g]	solid	490, 518 (365) 484, 518, 555_{sh}	13	20.1	6.5×10^3	4.3×10^4	500, 537 476, 515, 547	70.0

[a] $k_r = \phi/\tau_{average}$. [b] $k_{nr} = (1 - \phi)/\tau_{average}$. [c] ground solid (crystals obtained from CH_2Cl_2/*n*-hexane, **1a**: 538 nm, 298 K; 520, 545 nm, 77 K; **1c**: 485, 515, 555 nm, 298 K; 485, 525, 570 nm, 77 K; [d] Identical profile at 10^{-4} M and at 10^{-3} M, [e] The band at 370 nm disappears in concentrated solution (10^{-3}M) due to self absorption. [f] Non emissive. [e] Ref 11b

Table 4 Cytotoxic IC_{50} values (μM) and fluorescence cellular localization of **3a**, **3b**, **4** and cisplatin in human lung cell lines A549 (adenocarcinomic alveolar basal epithelial cells) and NL20 (immortalized non-tumorigenic bronchial epithelial cells).

Complex	**A549**		**NL20**	
	IC_{50} [¶]	**Cellular localization**	**IC_{50}** [¶]	**Cellular localization**
3a	24.70 ± 0.38	Cytoplasm (perinuclear), nucleus (condensed DNA) and nucleolus	10.45 ± 0.24	Cytoplasm (perinuclear), and nucleolus
3b	23.46 ± 2.78	Cytoplasm (perinuclear)	11.13 ± 0.09	Cytoplasm (perinuclear)
4	18.92 ± 0.36	Cytoplasm (perinuclear), nucleus and nucleolus	9.03 ± 0.29	Cytoplasm (perinuclear) and nucleolus
Cisplatin	6.45 ± 0.47	-	2.83 ± 0.36	-

[¶] IC_{50} values are presented as mean ± the standard error of the mean of three different experiments

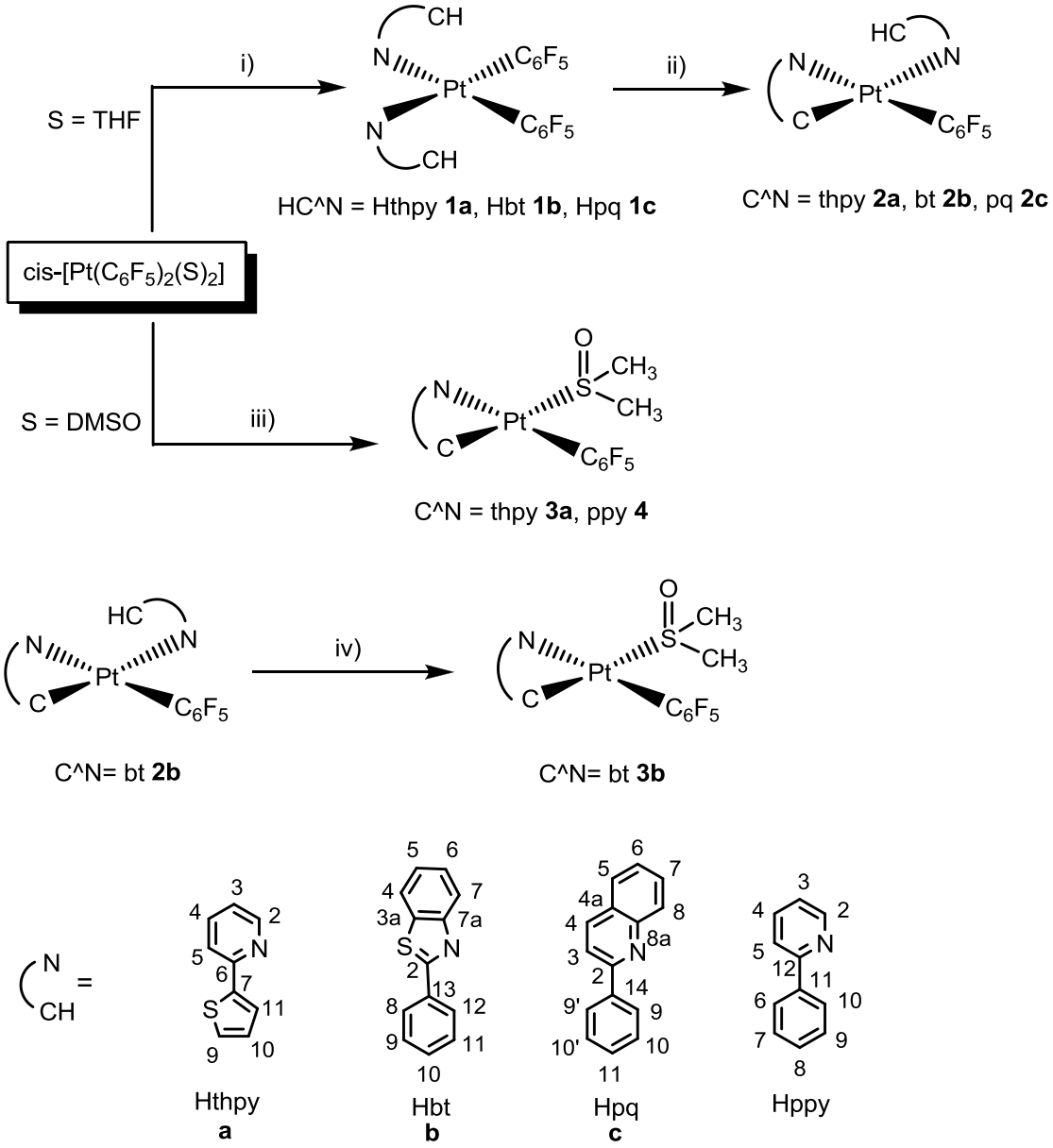

Scheme 1: i) HC^N (2 equiv), CH_2Cl_2, ii) xylene at reflux, iii) HC^N (1 equiv), xylene at reflux, iv) DMSO, reflux

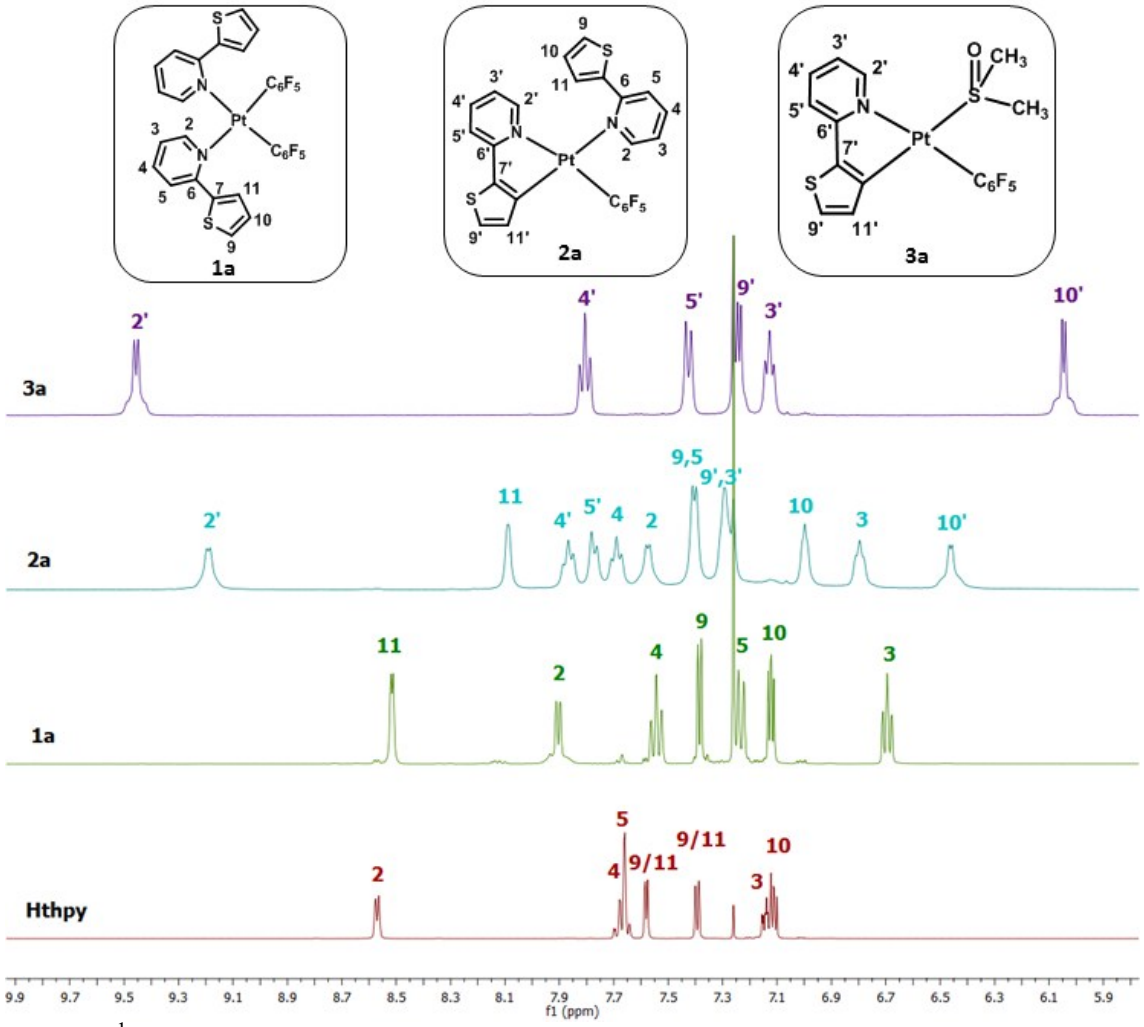

Fig. 1 ^{1}H NMR spectra of Hthpy, **1a**, **2a** and **3a** in $CDCl_3$ at 298 K

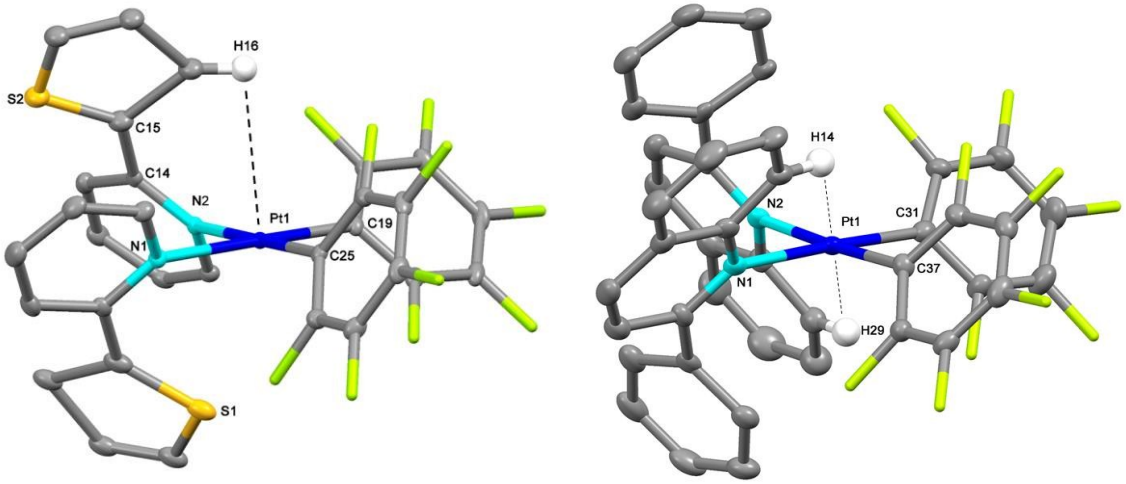

a) b)

Fig. 2 View of the molecular structure of a) **1a**, b) **1c**·0.75CH_2Cl_2

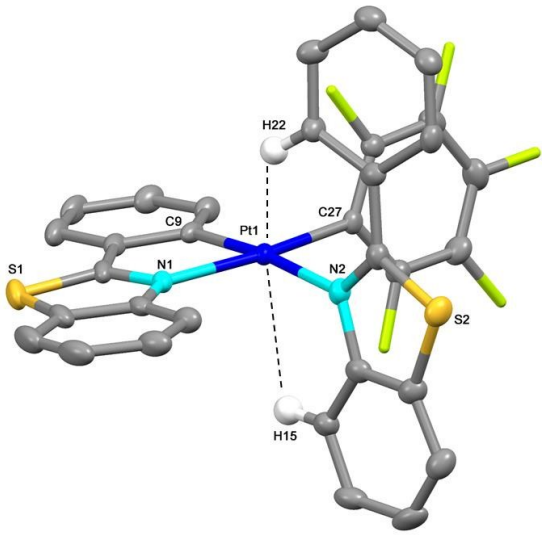

Fig. 3 Molecular structure of **2b**

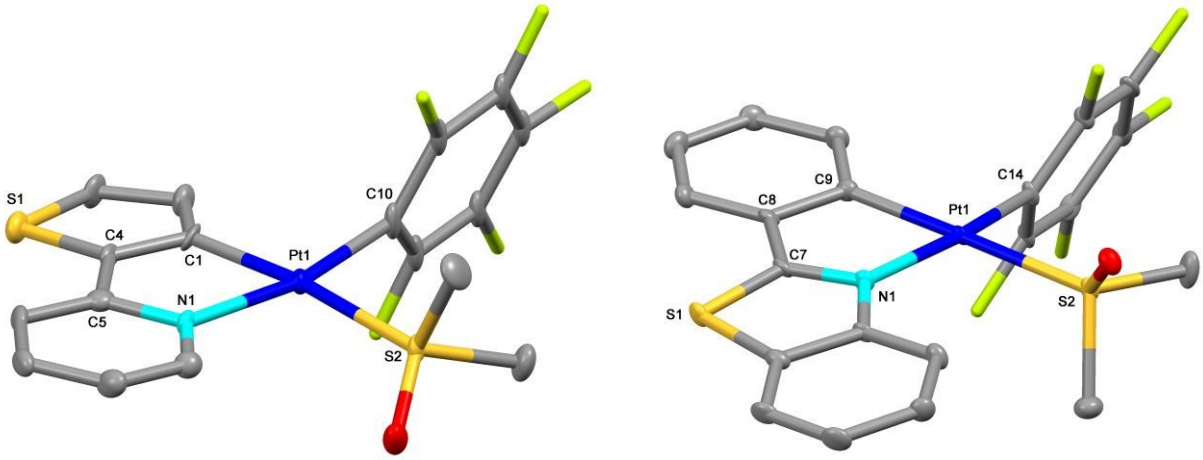

a) b)

Fig. 4 Molecular structures of a) **3a**, b) **3b**

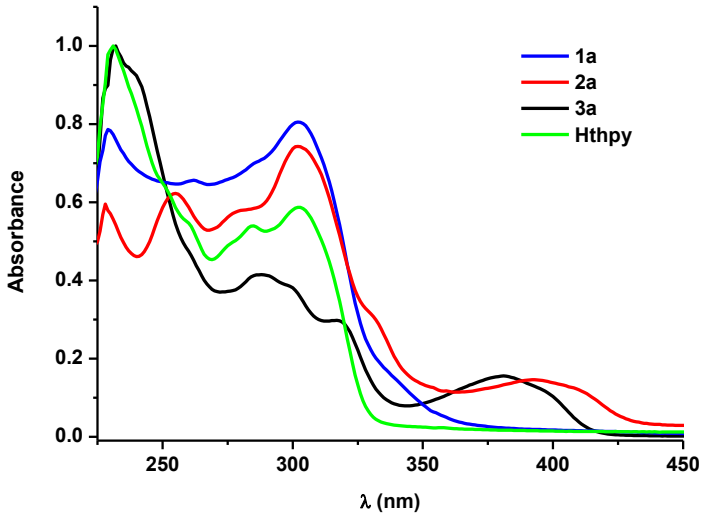

Fig. 5 Absorption spectra of the thpy series of complexes (**1a**, **2a** and **3a**) and the Hthpy ligand in CH_2Cl_2 (5 x 10^{-5} M) at 298 K.

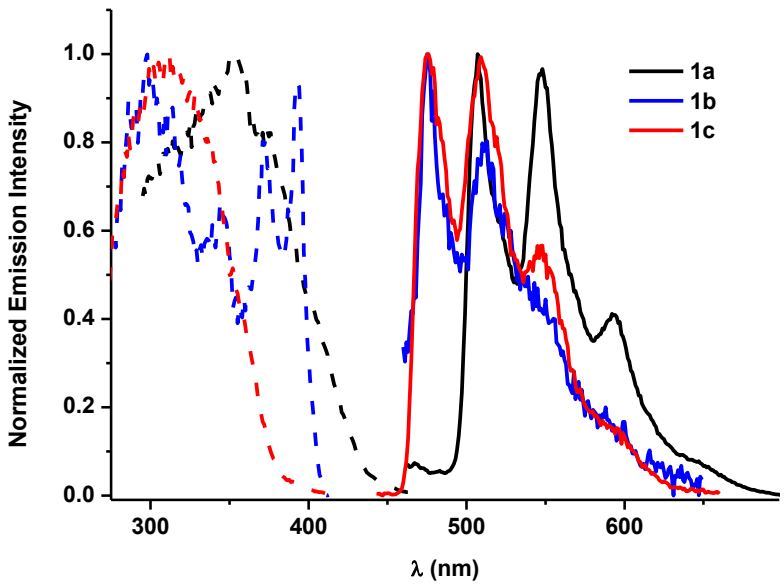

Fig. 6 Normalized excitation and emission spectra of **1a**, **1b** and **1c** in CH_2Cl_2 5 x 10^{-5} M at 77 K.

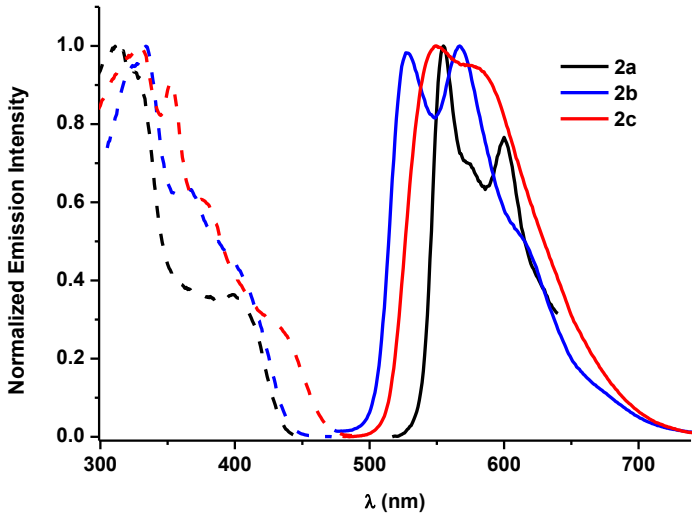

Fig. 7 Normalized excitation and emission spectra of **2a**, **2b** and **2c** in CH_2Cl_2 $5x10^{-5}$ M at 298 K (λ_{exc} 380-410 nm).

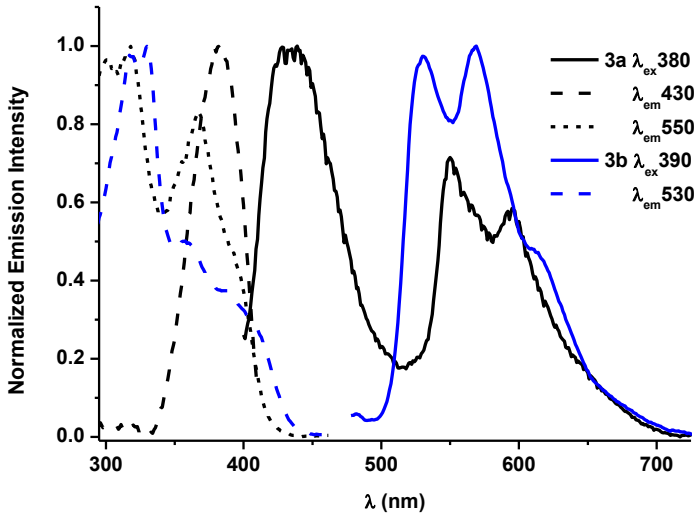

Fig. 8 Normalized excitation and emission spectra of **3a** and **3b** in CH_2Cl_2 $5x10^{-5}$ M at 298 K

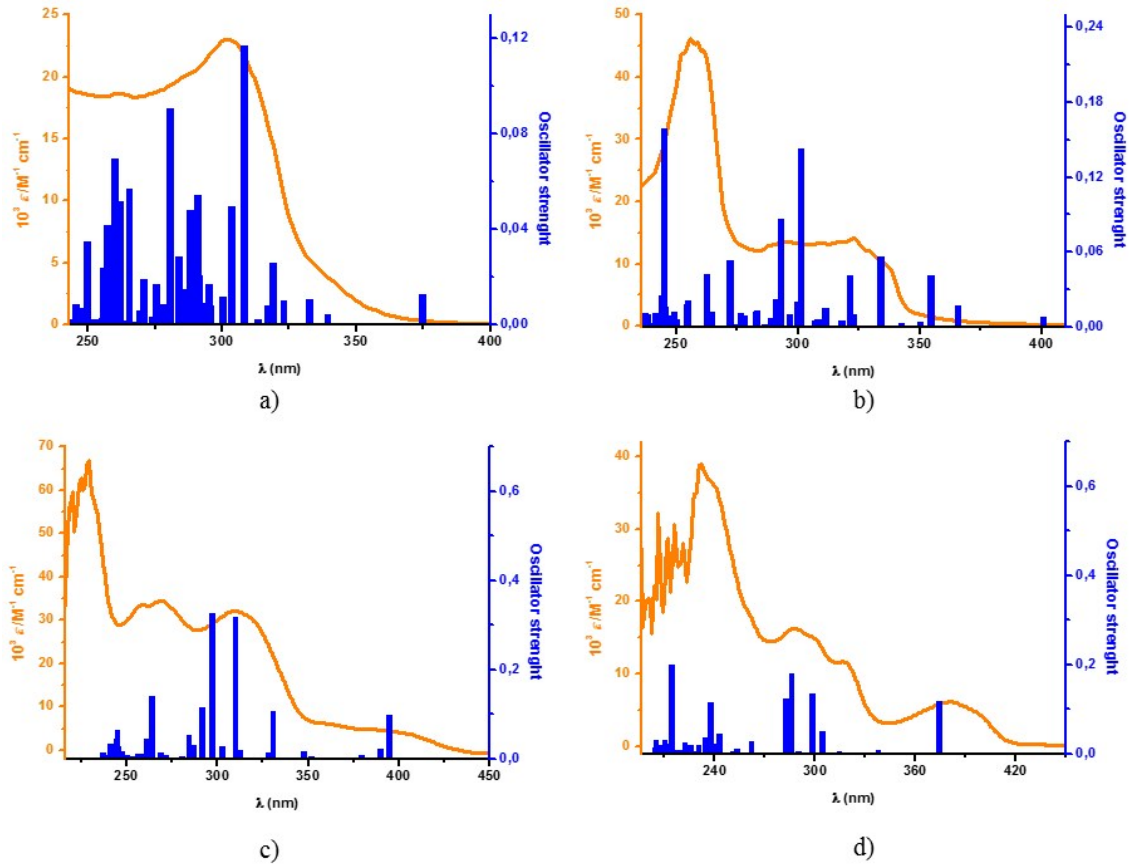

Fig.9 Calculated stick absorption spectra of a) **1a**, b) **1c**, c) **2b** and d) **3a** in CH_2Cl_2 compared with the experimental spectra

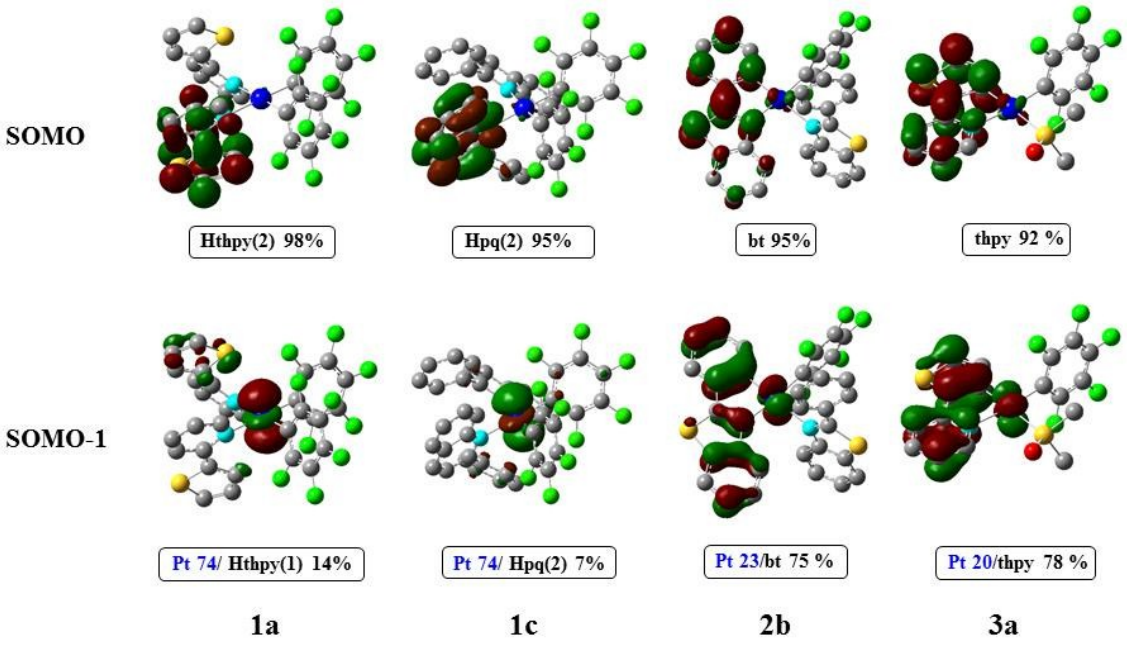

Fig. 10 SOMO and SOMO-1 of complexes **1a**, **1c**, **2b** and **3a**.

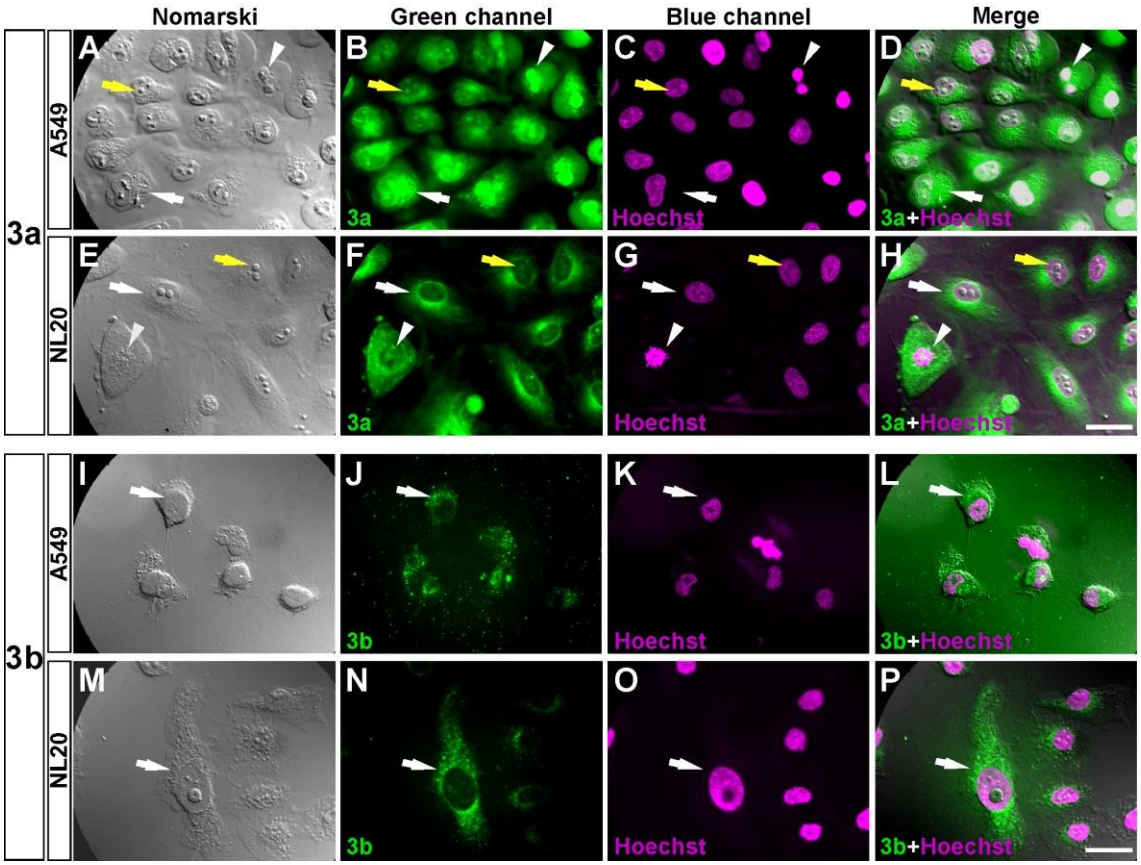

Fig. 11 Fluorescence images of A549 and NL20 cells treated with complexes **3a** and **3b.** Living cells were treated with complexes **3a** (A-H) or **3b** (I-P) (40 μM) mixed with the DNA binder Hoechst 33258 (3.2 μM) for 30 min. Cells were visualized by microscopy either for Nomarski white-light transmission (A, E, I and M), or fluorescence emission in green (B, F, J and N) and blue (C, G, K and O). Overlay of Nomarski, green and blue images are shown in right panels (D, H, L and P) (merged). Note that in A549 cells, **3a,** and with less intensity **3b,** stain the cytoplasm in green, with higher intensity in perinuclear areas (white arrows) in both cell lines. **3a,** but not **3b,** strongly stains nuclear condensed DNA (white arrowheads), and nucleoli (yellow arrows). In NL20 cells, **3a** stains the cytoplasm, stronger in perinuclear localization (white arroheads), and nucleoli (yellow arrows), but does not stain condensed DNA in nuclei (white arrowheads); **3b** only stains the cytoplasm with a punctuated pattern (white arrows). 3b Scales bar in H and P: 30 μm.

"for Table of Contents"

Strong luminescent pentafluorophenyl cyclometalated complexes have been synthesized. They have been fully characterized and their photophysical properties studied, supported by DFT TD-DFT calculations. The cytotoxicity of the solvate derivatives against the tumor A549 (lung carcinoma) and non-tumor NL20 (bronchial epithelial) cell lines have been evaluated. Fluorescent cell microscopy pointed out to their localization on the cytoplasm.